

Supporting Information

Balancing the Acidity of Pendant Urea Arm of Bis-Heteroleptic Ruthenium(II) Complex Containing Pyridyl Triazole for Improved Oxyanion Recognition

*Tamal Kanti Ghosh and Pradyut Ghosh**

**Department of Inorganic Chemistry, Indian Association for the Cultivation of Science, 2A & 2B Raja S. C. Mullick Road, Kolkata 700032, India, E-mail: icpg@iacs.res.in*

Contents

Topics	Page no.
Experimental Section	S1-S7
Spectral Characterization of all the compounds	S8-S19
Solution-state ¹H-NMR studies	S20-S28
ITC experiments	S29
Photophysical studies	S30-S33
Extraction studies with anions	S34-S36
References	S37

EXPERIMENTAL SECTION

Materials. Reactions were carried out either in the typical atmosphere or in argon gas atmosphere followed by workup at ambient conditions. Acetonitrile and dichloromethane were dried over CaH_2 and was collected before use whereas 99.9 % ethanol was used as received. HPLC grade CH_3CN was purchased from Spectrochem Pvt. Ltd., India and used for ITC and photophysical studies. $\text{RuCl}_3 \cdot \text{XH}_2\text{O}$, 1,10 phenanthroline, Deuterated solvents, tetrabutylammonium salts of F^- , Cl^- , Br^- , I^- , CH_3CO_2^- , PhCO_2^- , ClO_4^- , NO_3^- , HCO_3^- , HO^- , HSO_4^- , H_2PO_4^- , and $\text{HP}_2\text{O}_7^{3-}$ were purchased from Sigma-Aldrich and were used as received.

Methods. The sample for mass spectrometry for complex $\mathbf{1}[\text{PF}_6]_2$ and $\mathbf{2}[\text{PF}_6]_2$ was prepared by dissolving the compound in acetonitrile having a concentration $\approx 2 \times 10^{-6}(\text{M})$. High-resolution ESI-MS experiments were carried out with a Waters QtoF Model YA 263 mass spectrometer in positive ESI mode. Elemental analysis was performed on PerkinElmer 2500 series II elemental analyzer, PerkinElmer, USA. NMR experiments were carried out with FT-NMR Bruker DPX 500/400/300 MHz NMR spectrometer. The absorption and emission studies were performed in a PerkinElmer Lambda 900 UV-Vis-NIR spectrometer (NIR = near-infrared) (with a quartz cuvette of path length 1 cm) and FluoroMax-3 spectrophotometer, from Horiba Jobin Yvon, respectively. For the time-correlated single photon counting (TCSPC) measurements, samples were excited at 400 nm using picoseconds diode laser (IBH Nanoled-07) in an IBH Fluoro-cube apparatus. The luminescence decay data were recorded on a Hamamatsu MCP photomultiplier (R3809) and were analyzed using IBH DAS6 software. Chemical shifts for ^1H and ^{13}C NMR were reported in parts per million (ppm), calibrated to the residual solvent peak set, with coupling constants reported in Hertz (Hz).

Isothermal Titration Calorimetric (ITC) Studies: The isothermal titration calorimetric (ITC) experiments were performed with a Micro-Cal VP-ITC instrument using HPLC grade CH₃CN solvent at 298K. A solution of the host in CH₃CN was kept in the measuring cell and titrated with 30 injections of the respective guest solution (10 μL per addition) in CH₃CN. An interval of 220 seconds was allowed between each injection, and the stirring speed was set at 329 rpm. The titration data were processed by using Origin 7.0 software, supplied with the instrument. All the titration data were fitted to either one site or sequential site binding model as applicable. Reference titrations with only solvents were also performed and subtracted from the corresponding titration to remove any effect from the heats of dilution from the titrant.

Extraction Details: In the course of liquid-liquid extraction, complex **1**[PF₆]₂/2[PF₆]₂ were taken in CHCl₃, and an aqueous solution of respective anions were added into it to form two immiscible layers which were stirred vigorously for 5-6 hours. Then, the organic layer was separated and dried by passing through Na₂SO₄. Finally, the organic layer was concentrated, and diethyl ether was added to obtain the extracted product. Extracted products were analyzed by NMR and extraction efficiency of complexes were calculated by using 1,3,5 trimethoxybenzene (TMB) as an internal standard.¹

Following equation was used for calculation of extraction efficiency:

$$\text{Efficiency in percentage (\%)} = \left[\frac{\text{area under urea - NH proton peak}}{(\text{area under aromatic - CH proton peak of TMB}/3)} \right] \times 100$$

Syntheses:

Synthesis of tert-butyl (2-azidoethyl) carbamate and tert-butyl (2-(4-(pyridin-2-yl)-1H-1,2,3-triazol-1-yl)ethyl) carbamate: These compounds were prepared as reported previously.²

Synthesis of 1-(1-naphthyl)-3-(2-(4-(pyridin-2-yl)-1H-1,2,3-triazol-1-yl)ethyl)urea (L1): 202 mg (0.698 mmol) tert-butyl (2-(4-(pyridin-2-yl)-1H-1,2,3-triazol-1-yl)ethyl) carbamate was taken in a RB flux and dissolved in 20 ml DCM. Excess CF₃COOH (2 ml) in 10 ml DCM was added dropwise into the RB at ~0°C. The reaction mixture was allowed to stir for ≈ 2 hours before all the volatiles were evaporated. After that, 15 ml dry DCM was added to this reaction mixture and 0.971 ml dry Et₃N (6.98 mmol) was added. The reaction mixture was allowed to stir for next 10 minutes at room temperature. Finally, 100 μL 1-naphthyl isocyanate (0.698 mmol) in 10 ml dry DCM was added dropwise into the reaction mixture *via* a pressure equalizing funnel at 0°C. Immediate appearance of precipitate was observed which was allowed to stir for 6 hours. After that the solution was filtered and washed for several with water and di-ethyl ether and dried overnight to yield the desired product, **L1** as white solid (215 mg, 87% yield). Anal. calcd. for **L1**, C₂₀H₁₈N₆O (MW = 358.39) C, 67.02; H, 5.06; N, 23.45; found: C, 66.88; H, 4.77; N, 23.98%. ESI-MS [**L1+H**]⁺: calcd, m/z = 359.1620; found, m/z = 359.2456, [**L1+Na**]⁺: calcd, m/z = 381.1440; found, m/z = 381.2395; ¹H-NMR (300 MHz, DMSO-*d*₆): δ = 8.64 (s, 1H), 8.61-8.58 (m, 2H), 8.07-8.04 (m, 1H), 8.01-7.86 (m, 4H), 7.58-7.32 (m, 5H), 6.70-6.67 (t, 1H, 6 Hz), 4.61-4.57 (t, 2H, 6 Hz), 3.73-3.67 (dd, 2H) ppm. ¹³C NMR (75 MHz, DMSO-*d*₆): δ = 155.7, 150.1, 149.6, 147.4, 149.6, 147.3, 137.3, 134.9, 133.7, 128.3, 126.0, 125.9, 125.8, 125.5, 123.6, 123.0, 122.6, 121.6, 119.6, 117.3, 50.1, 39.1 ppm.

Synthesis of 1-(pentafluorophenyl)-3-(2-(4-(pyridin-2-yl)-1H-1,2,3-triazol-1-yl)ethyl)urea (L2): 200 mg (0.643 mmol) tert-butyl (2-(4-(pyridin-2-yl)-1H-1,2,3-triazol-1-yl)ethyl) carbamate

was taken in a RB flask and dissolved in 20 ml DCM. Excess CF₃COOH (2 ml) in 10 ml DCM was added drop wise into the RB at ~0°C. The reaction mixture was allowed to stir for ≈ 2 hours before all the volatiles were evaporated. After that, 15 ml dry DCM was added to this reaction mixture and 0.894 ml dry Et₃N (6.43 mmol) was added. The reaction mixture was allowed to stir for next 10 minutes at room temperature. Then, 84 μL pentafluorophenyl isocyanate (0.643 mmol) in 10 ml dry DCM was added drop wise into the reaction mixture *via* a pressure equalizing funnel at 0°C. The solution was allowed to stir for 6 hours. After that, the solution was evaporated and the water was added to the mixture. Immediate formation of a precipitate was observed which was filtered and washed for several times with water and di-ethyl ether and dried overnight to yield the desired product, **L2** as light brown solid (231 mg, 91% yield). Anal. calcd. for **L2**, C₁₆H₁₁F₅N₆O (MW = 398.29) C, 48.25; H, 2.78; N, 23.85; found: C, 48.21; H, 2.54; N, 22.78%. ESI-MS [**L2**+H]⁺: calcd, m/z = 399.0993; found, m/z = 398.9958, [**L2**+Na]⁺: calcd, m/z = 421.0812; found, m/z = 420.9646; ¹H-NMR (300 MHz, DMSO-*d*₆): δ = 8.60-8.57 (m, 2H), 8.42 (s, 1H), 8.03-8.00 (m, 1H), 7.91-7.86 (m, 1H), 7.36-7.31 (m, 1H), 6.75-6.72 (t, 1H, 6 Hz), 4.54-4.50 (t, 2H, 6.6 Hz), 3.65-3.60 (dd, 2H) ppm. ¹³C NMR (75 MHz, DMSO-*d*₆): δ = 154.5, 150.1, 149.6, 147.3, 144.3, 141.2, 138.7, 137.2, 135.6, 123.5, 122.9, 119.4, 114.5, 49.6, 39.5 ppm.

Synthesis of complex 1[PF₆]₂: *cis*-[Ru(Phen)₂Cl₂] was synthesized as reported in literature³ and used as a starting material for the synthesis of complex. *cis*-[Ru(Phen)₂Cl₂] (222 mg, 0.42 mmol) and **L1** (150 mg, 0.42 mmol) and were dissolved in 30 mL of well-degassed ethanol-water binary solvent mixture (2:1; v/v). The mixture was heated to reflux under argon atmosphere for 48 hours until the color of the solution became dark red. After that the reaction mixture was cooled to room temperature and ethanol was evaporated. Remaining aqueous solution was

treated with excess KPF_6 salt dissolved in water. Orange-red precipitate was formed immediately after addition which was filtered, washed with water, and dried under vacuum to get the desired complex $\mathbf{1}[\text{PF}_6]_2$ as orange-red crystalline solid (301 mg, 65% yield). Anal. calcd. for $\mathbf{1}[\text{PF}_6]_2$, $\text{C}_{44}\text{H}_{34}\text{F}_{12}\text{N}_{10}\text{OP}_2\text{Ru}$ (MW = 1109.81) C, 47.62; H, 3.09; N, 12.62; found: C, 48.30; H, 2.69; N, 12.92%. ESI-MS [$\mathbf{1}[\text{PF}_6]_2 - \text{PF}_6^- = \text{C}_{44}\text{H}_{34}\text{F}_6\text{N}_{10}\text{OPRu}^+$]: calcd, m/z = 965.1602; found, m/z = 965.2625; ^1H NMR (300 MHz, $\text{DMSO}-d_6$): δ = 9.50 (s, 1H, $-\text{CH}_a$), 8.85 (s, 1H, $-\text{NH}_b$), 8.83–8.79 (t, 2H), 8.74–8.73 (d, 1H), 8.66–8.65 (d, 1H), 8.56–8.55 (d, 1H), 8.41–8.30 (m, 6H), 8.07–8.03 (m, 2H), 7.96–7.93 (m, 2H), 7.87–7.84 (m, 1H), 7.74–7.72 (m, 1H), 7.62–7.59 (m, 1H), 7.53–7.52 (d, 1H), 7.29–7.23 (m, 3H), 6.97–6.93 (t, 2H), 6.54 (t, 1H, $-\text{NH}_c$), 4.46–4.34 (m, 2H), 3.57–3.28 (m, 2H) ppm. ^{13}C NMR (75 MHz, $\text{DMSO}-d_6$): δ = 159.1, 156.1, 155.9, 153.6, 153.3, 153.2, 152.2, 151.2, 148.2, 147.9, 147.8, 147.7, 138.8, 137.4, 136.9, 136.8, 130.9, 130.8, 130.4, 128.5, 127.3, 126.9, 126.7, 126.1, 122.8, 120.6, 120.5, 115.7, 115.4, 55.4, 53.3 ppm.

Synthesis of complex $\mathbf{2}[\text{PF}_6]_2$: *cis*- $[\text{Ru}(\text{Phen})_2\text{Cl}_2]$ (200 mg, 0.38 mmol) and **L2** (148 mg, 0.38 mmol) and were dissolved in 30 mL of well-degassed ethanol-water binary solvent mixture (2:1; v/v). The mixture was heated to reflux under argon atmosphere for 48 hours until the color of the solution became dark red. After that the reaction mixture was cooled to room temperature and ethanol was evaporated. Remaining aqueous solution was treated with excess KPF_6 salt dissolved in water. Orange-red precipitate was formed immediately after addition which was filtered, washed with water, and dried under vacuum to get the desired complex $\mathbf{2}[\text{PF}_6]_2$ as orange-red crystalline solid (306 mg, 71% yield). Anal. calcd. for $\mathbf{2}[\text{PF}_6]_2$, $\text{C}_{40}\text{H}_{27}\text{F}_{17}\text{N}_{10}\text{OP}_2\text{Ru}$ (MW = 1149.70) C, 41.79; H, 2.37; N, 12.18; found: C, 42.88; H, 2.76; N, 11.61%. ESI-MS [$\mathbf{2}[\text{PF}_6]_2 - \text{PF}_6^- = \text{C}_{40}\text{H}_{27}\text{F}_{11}\text{N}_{10}\text{OPRu}^+$]: calcd, m/z = 1005.0975; found, m/z = 1005.2207; ^1H NMR (300 MHz, $\text{DMSO}-d_6$): δ = 9.284 (s, 1H, $-\text{CH}_a$), 8.84–8.59 (m, 6H), 8.39–8.33 (m, 6H),

8.09–7.97 (m, 4H), 7.76–7.37 (m, 2H), 7.52–7.48 (m, 2H), 7.32–7.23 (m, 1H), 6.87–6.83 (t, 1H) ppm; ^{13}C NMR (75 MHz, DMSO- d_6): δ = 154.9, 153.6, 152.8, 152.7, 151.6, 150.9, 147.7, 147.4, 147.3, 147.2, 138.2, 136.9, 136.8, 136.6, 136.5, 130.5, 130.4, 130.0, 128.1, 128.0, 127.9, 126.9, 126.4, 126.3, 126.0, 122.4, 52.7 ppm.

Calculation of Binding Constant

Several chemical properties like emission intensity, change in chemical shifts were altered upon addition of anions into the solution of Complex $\mathbf{1}[\text{PF}_6]_2/2[\text{PF}_6]_2$, which was utilized for calculating the binding constants. Binding constant values between complex $\mathbf{1}[\text{PF}_6]_2/2[\text{PF}_6]_2$ with H_2PO_4^- and $\text{HP}_2\text{O}_7^{3-}$ were calculated from ^1H -NMR, UV-Vis and PL titration experiments. The binding constant values were calculated from ^1H -NMR titration data using WINEQNMR2 software⁴ for both 1:1 and 1:2 (host: guest) binding stoichiometry. The following equation was for calculating the binding constant from PL titration experiments by the non-linear fitting method:

For 1:1 (host: guest) binding stoichiometry we have used the following equation⁵

$$\Delta X = \left(\frac{X}{2 * H} \right) * \left\{ \left(G_0 + H_0 + \frac{1}{K} \right) - \sqrt{\left(G_0 + H_0 + \frac{1}{K} \right)^2 + 4G_0H_0} \right\}$$

Where G_0 and H_0 are the initial concentration of guest and host respectively, K is the binding constant and ΔX is the change in emission intensity for each addition of guest species.

For 1:2 (host: guest) binding stoichiometry the following equation was used²

$$\Delta X = \frac{X_{\Delta HG1}K_1[H]_0[G] + X_{\Delta HG2}K_1K_2[H]_0[G]^2}{1 + K_1[G] + K_1K_2[G]^2}$$

Where $[H]_0$ is the initial concentration of host, K_1 and K_2 are the stepwise association constants, and ΔX is the change in emission intensity.

Calculation of Detection Limit: The following equation was used for calculation of Detection limit (DL),

$$DL = \frac{(3 \times \text{standard deviation})}{\text{Slope}}$$

The slope was calculated from the linear fit plot of the change in emission intensity vs. concentration of the anion. SD corresponds to the standard deviation of the value of luminescence intensity the blank sample, measured for 15 consecutive blank samples.

Calculation of Excited state lifetime: For analysis of experimental time-resolved luminescence decays, the following equation was used:

$$P(t) = b + \sum_{i=1}^{i=n} a_i \exp(-t/\tau_i)$$

Where $P(t)$ is the decay, n is the number of discrete emissive species, b is a baseline correction factor, a_i is a pre-exponential factor, and τ_i is the excited-state luminescence lifetimes associated with the i^{th} component.

Following equation was used to calculate the average lifetime $\langle \tau \rangle$ in case of multi-exponential decays:⁶

$$\langle \tau_i \rangle = \sum a_i * \tau_i$$

Where a_i is the contribution from the i^{th} component.

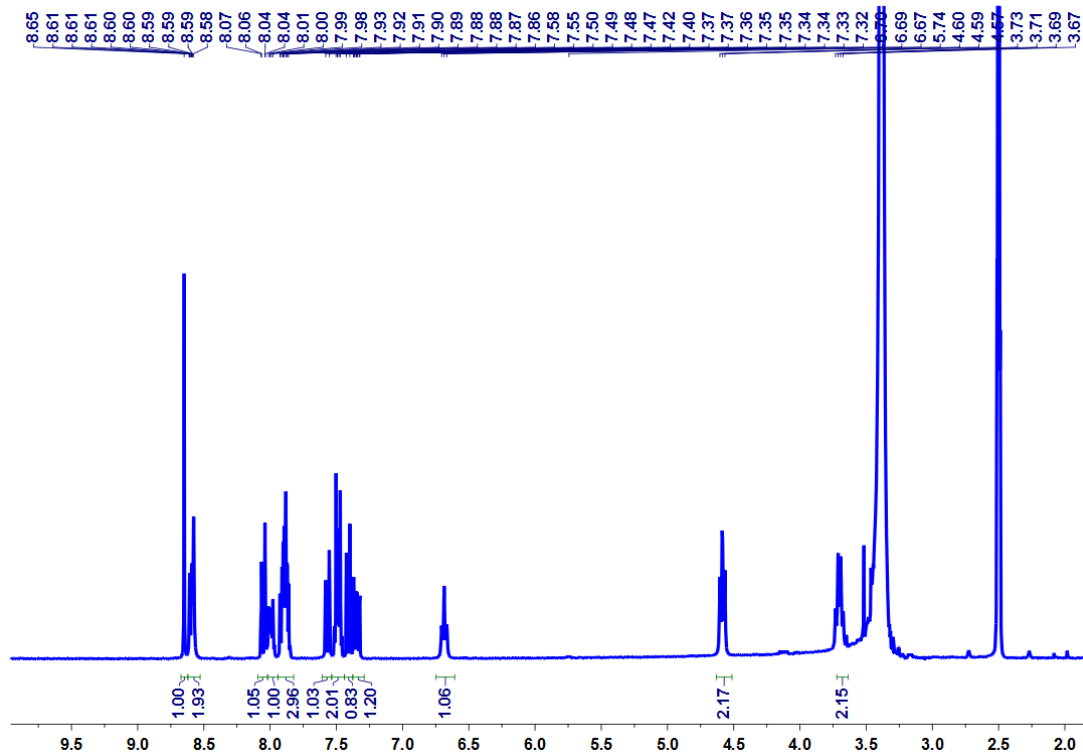


Figure S1. ^1H -NMR spectrum of **L1** in $\text{DMSO-}d_6$ in 300 MHz at 298K.

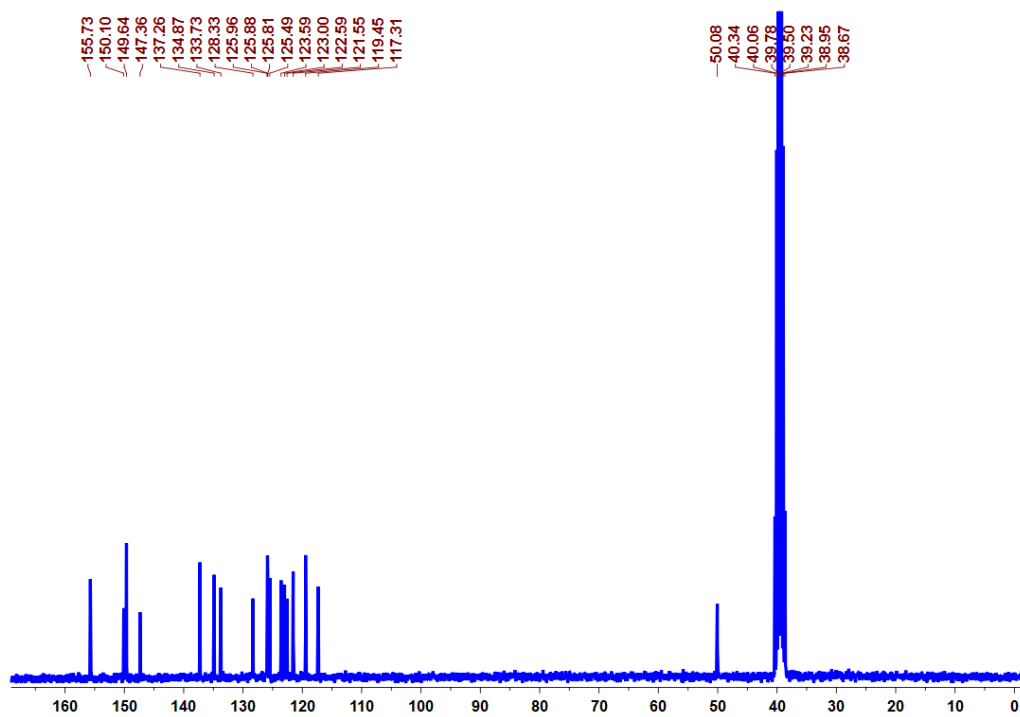


Figure S2. ^{13}C -NMR spectrum of **L1** in $\text{DMSO-}d_6$ in 75 MHz at 298K.

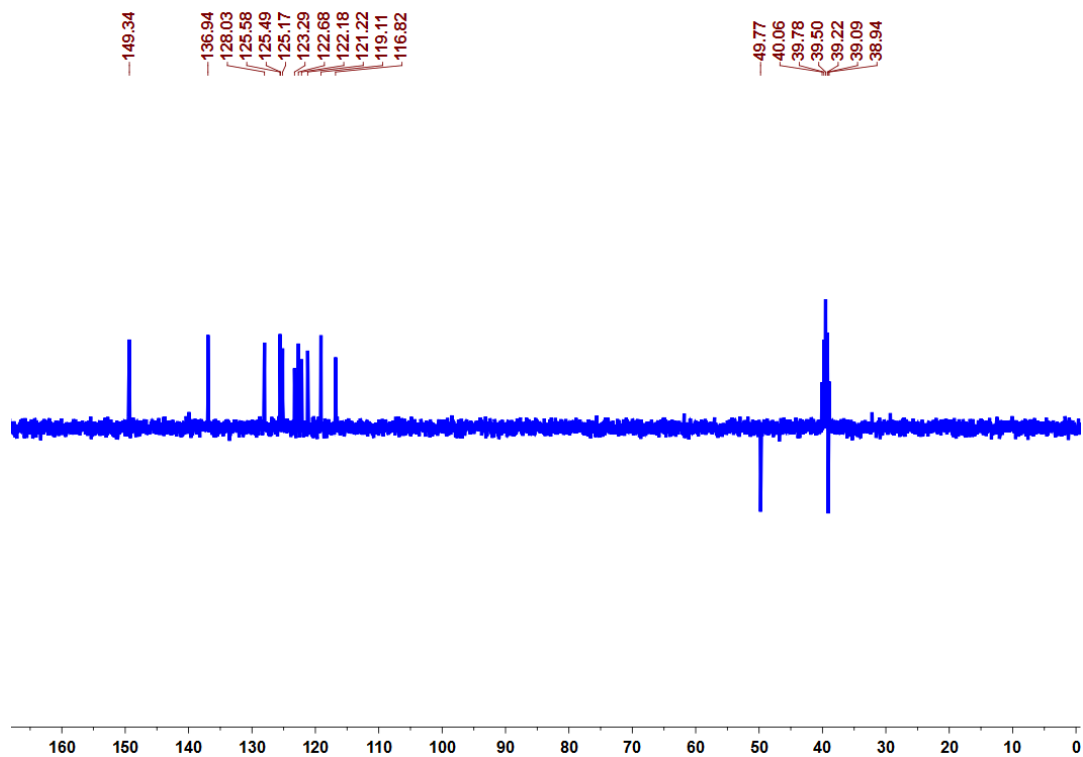


Figure S3. ^{13}C -DEPT-135 spectrum of **L1** in $\text{DMSO-}d_6$ in 75 MHz at 298K.

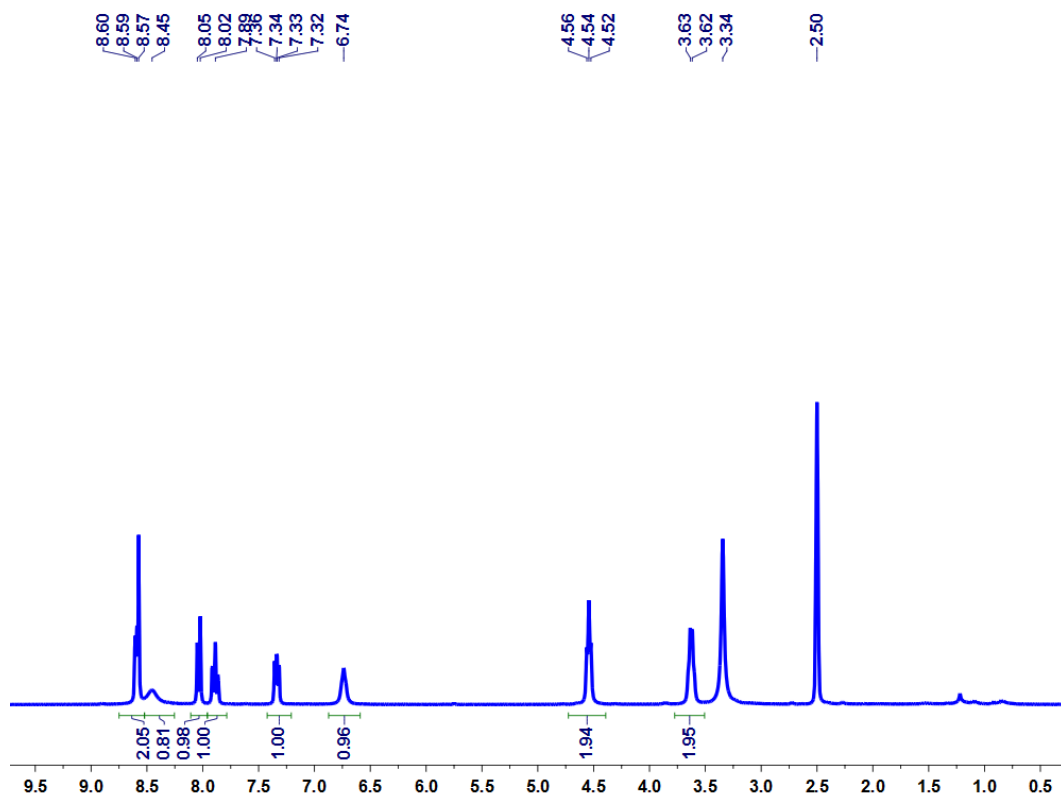


Figure S4. ^1H -NMR spectrum of **L2** in $\text{DMSO-}d_6$ in 300 MHz at 298K.

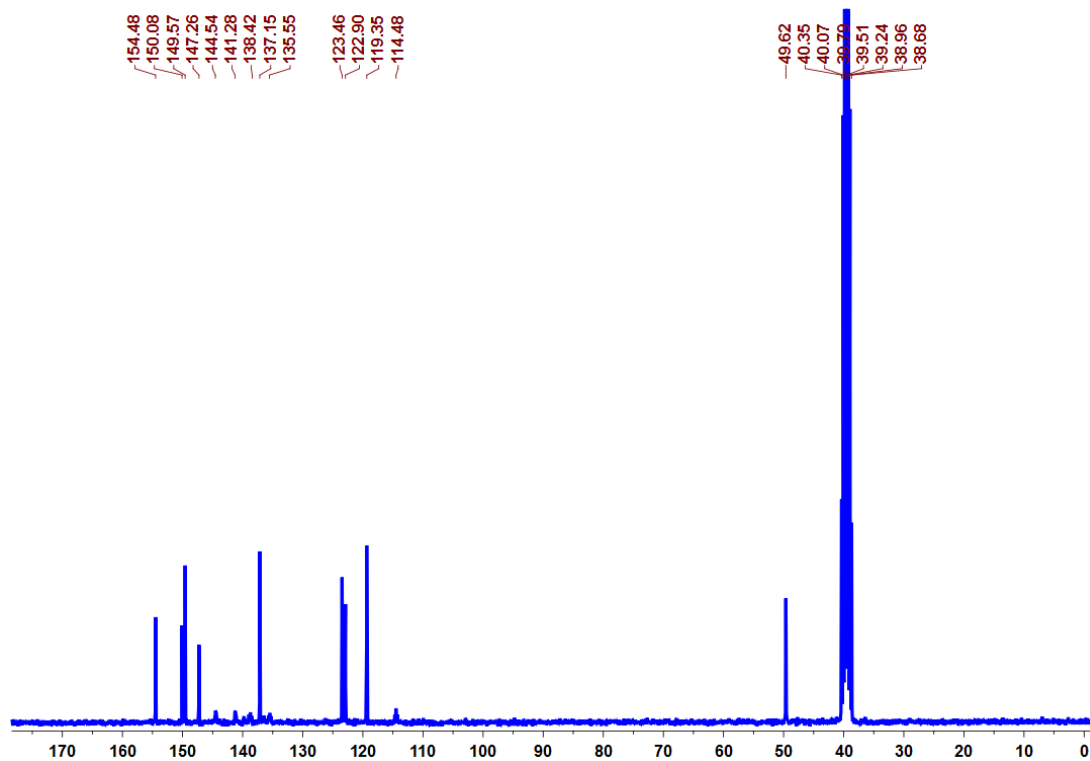


Figure S5. ^{13}C -NMR spectrum of **L2** in $\text{DMSO-}d_6$ in 75 MHz at 298K.

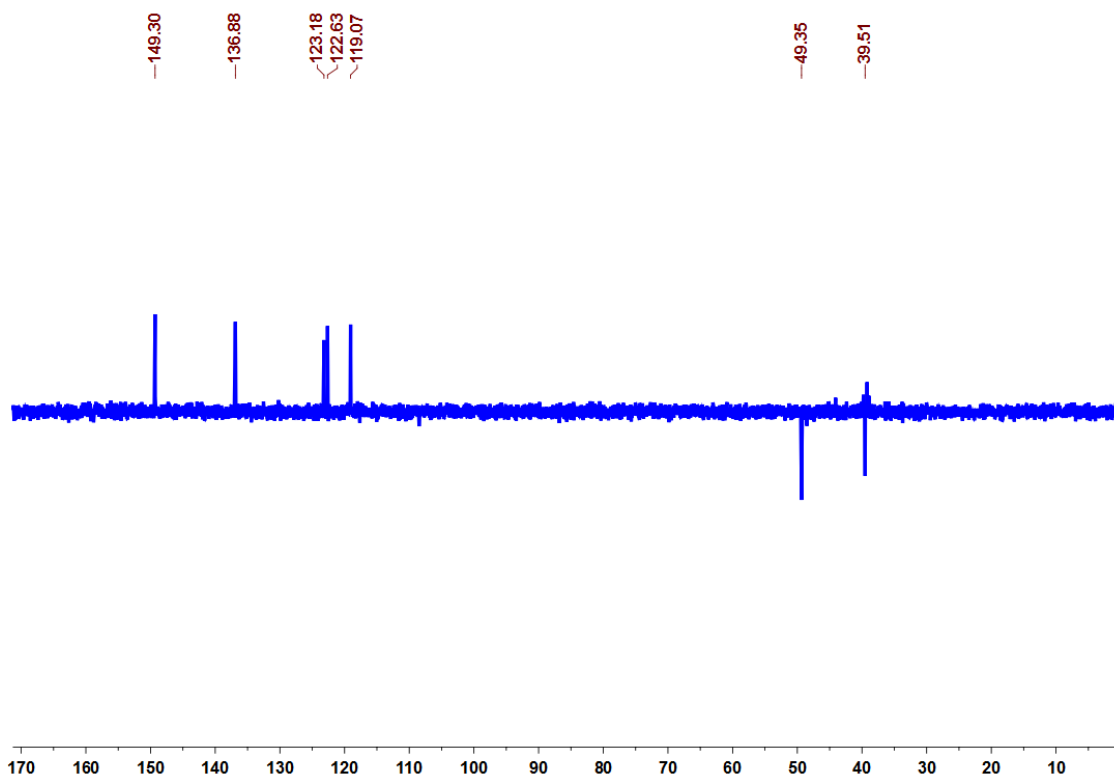


Figure S6. ^{13}C -DEPT-135 spectrum of **L2** in $\text{DMSO-}d_6$ in 75 MHz at 298K.

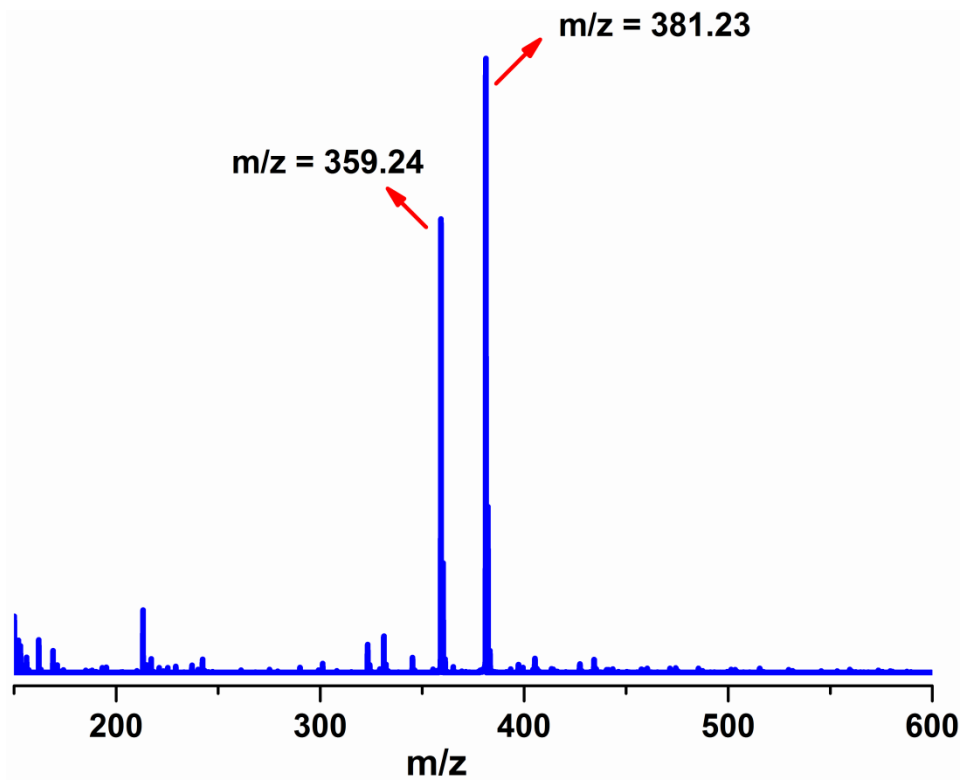


Figure SS6: ESI(+Ve) mass spectrum of L1 at 298K.

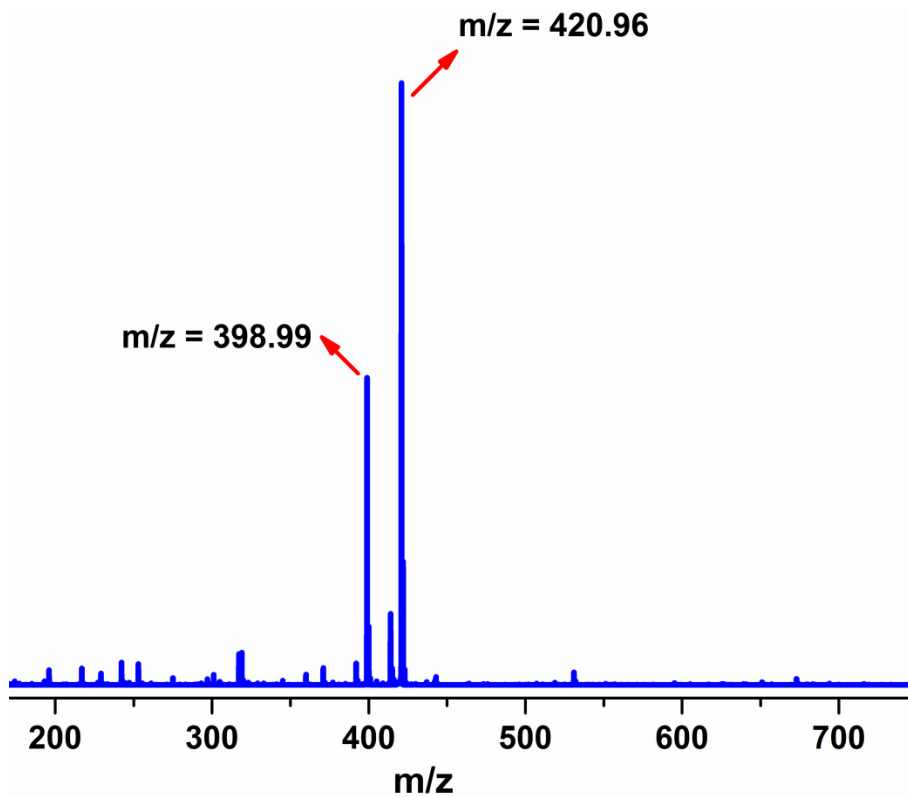


Figure SSS6: ESI(+Ve) mass spectrum of L2 at 298K.

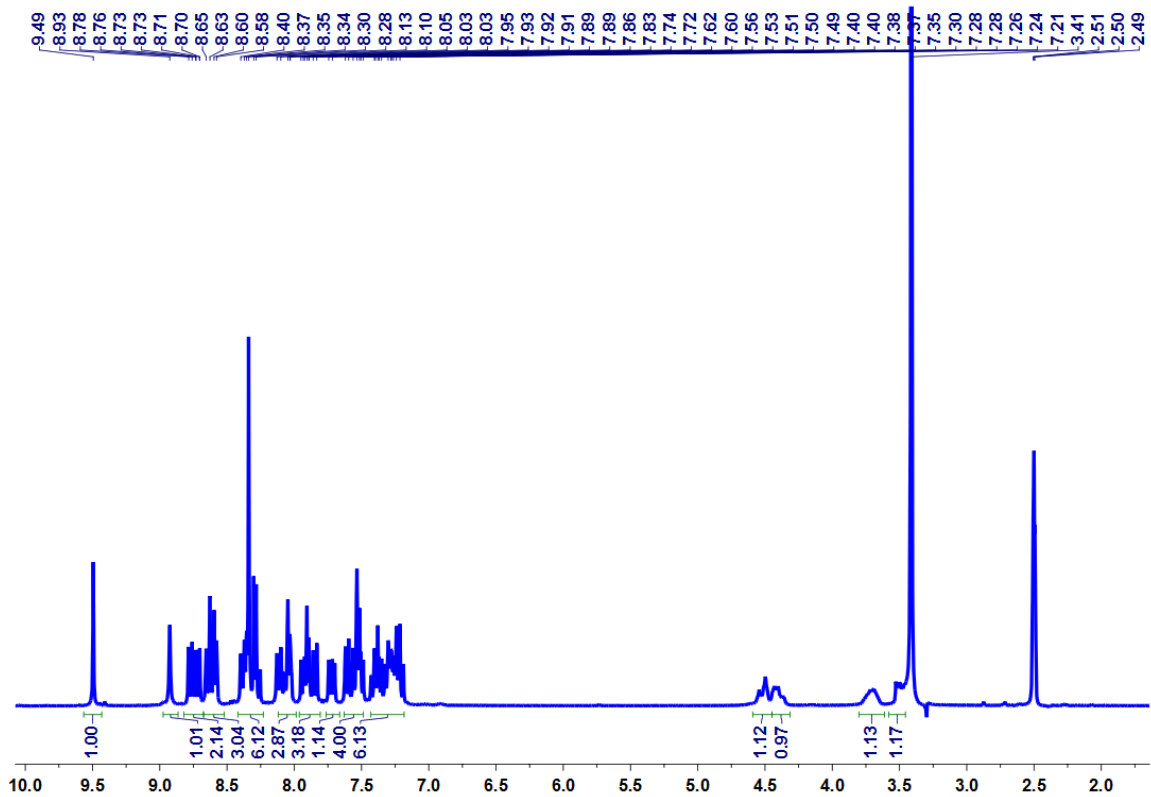


Figure S7. ^1H -NMR spectrum of $1[\text{PF}_6]_2$ in $\text{DMSO}-d_6$ in 300 MHz at 298K.

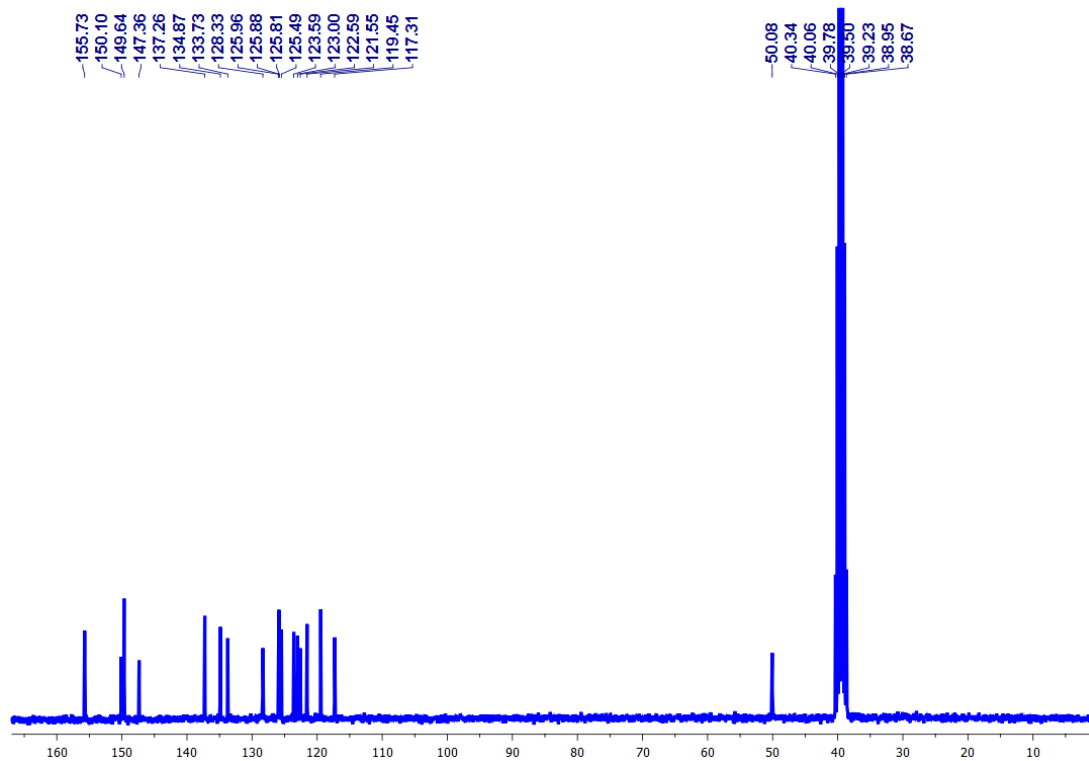


Figure S8. ^{13}C -NMR spectrum of $1[\text{PF}_6]_2$ in $\text{DMSO}-d_6$ in 75 MHz at 298K.

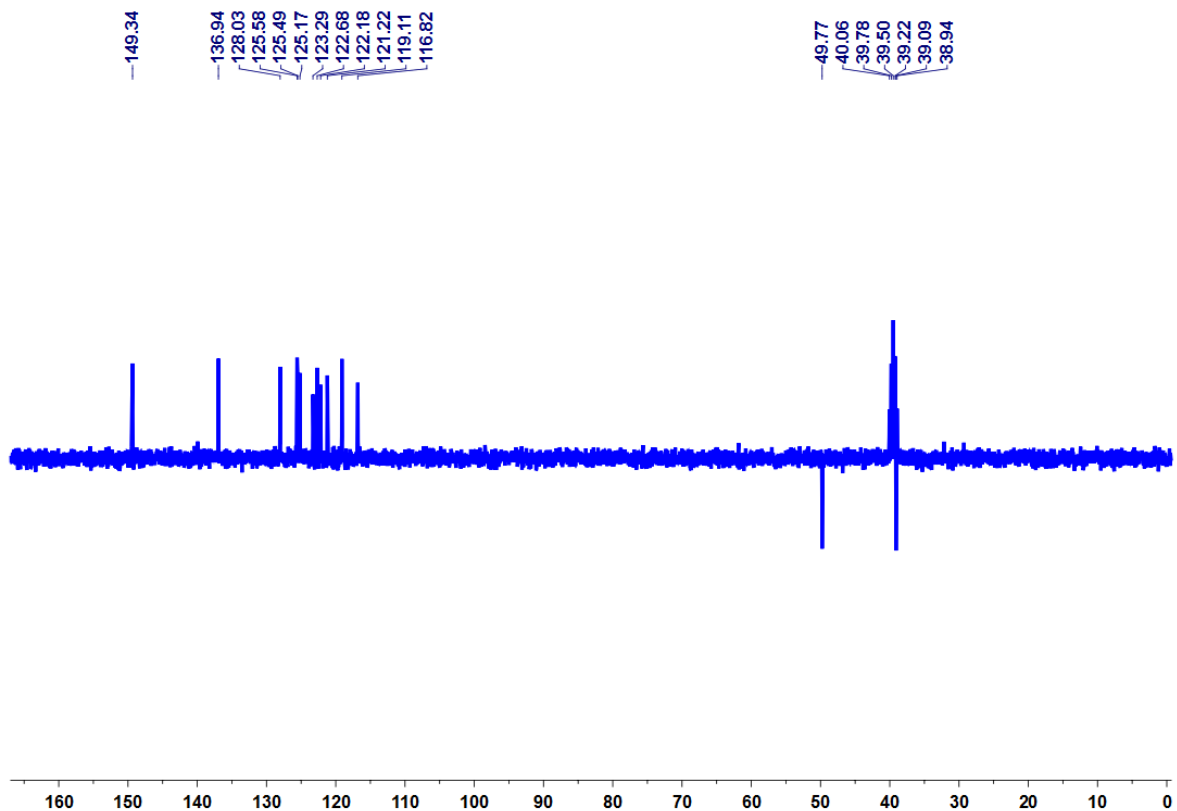


Figure S9. ^{13}C -DEPT-135 NMR spectrum of $1[\text{PF}_6]_2$ in $\text{DMSO-}d_6$ in 75 MHz at 298K.

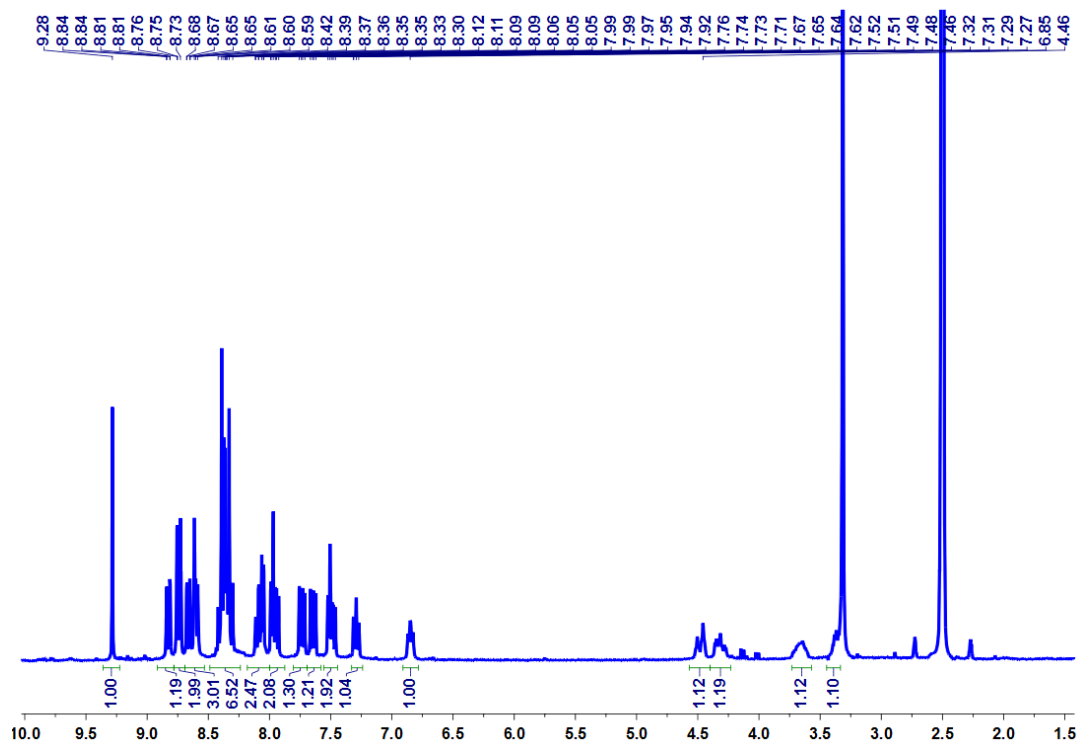


Figure S10. ^1H -NMR spectrum of $2[\text{PF}_6]_2$ in $\text{DMSO-}d_6$ in 300 MHz at 298K.

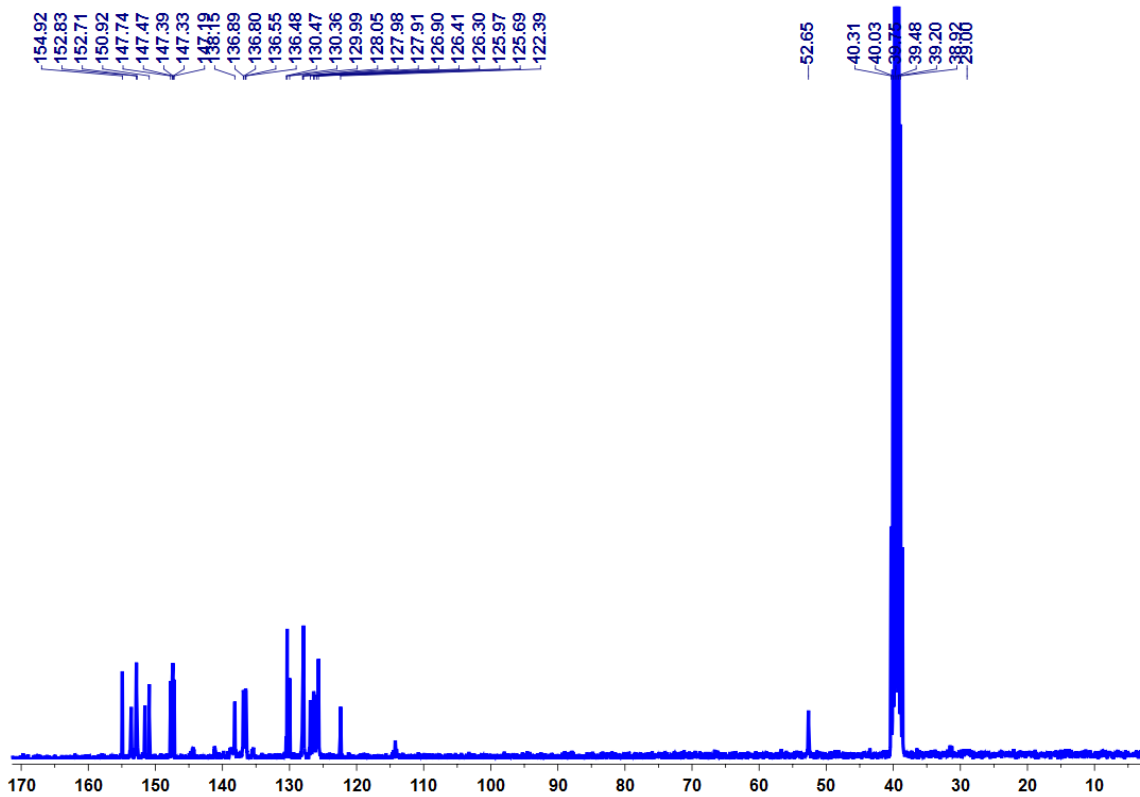


Figure S11. ^{13}C -NMR spectrum of $2[\text{PF}_6]_2$ in $\text{DMSO-}d_6$ in 75 MHz at 298K.

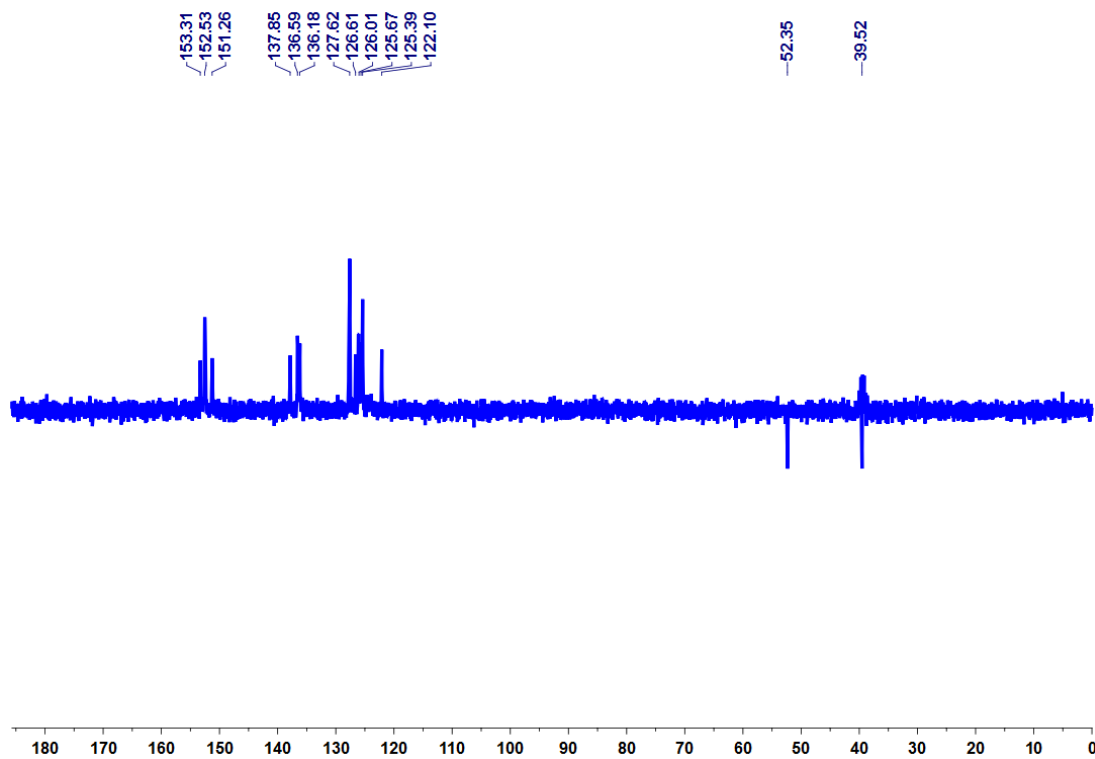


Figure S12. ^{13}C -DEPT-135 NMR spectrum of $2[\text{PF}_6]_2$ in $\text{DMSO-}d_6$ in 300 MHz at 298K.

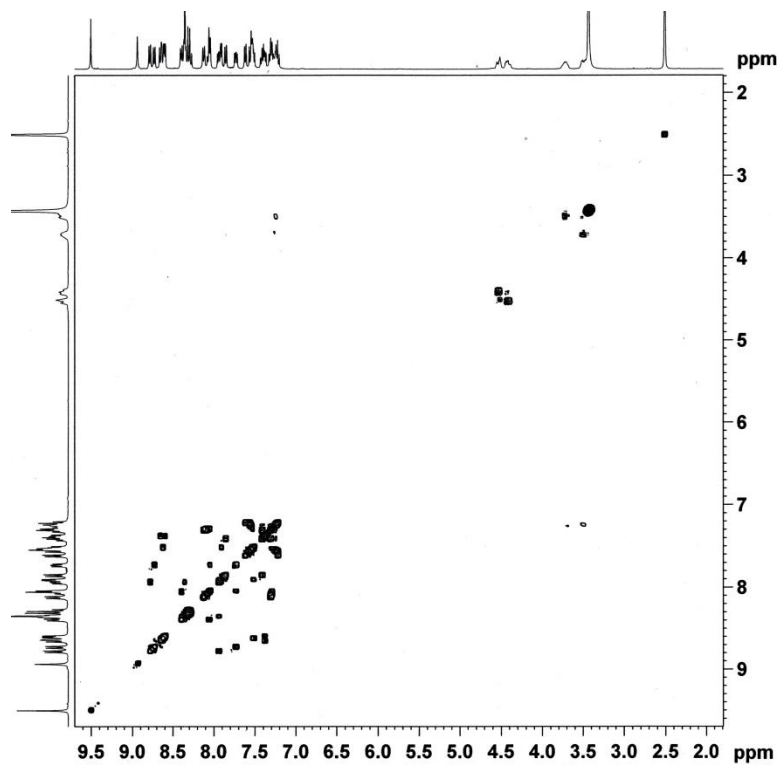


Figure S13. ^1H - ^1H COSY-NMR of complex $1[\text{PF}_6]_2$ in $\text{DMSO}-d_6$ at 298K in 500 MHz.

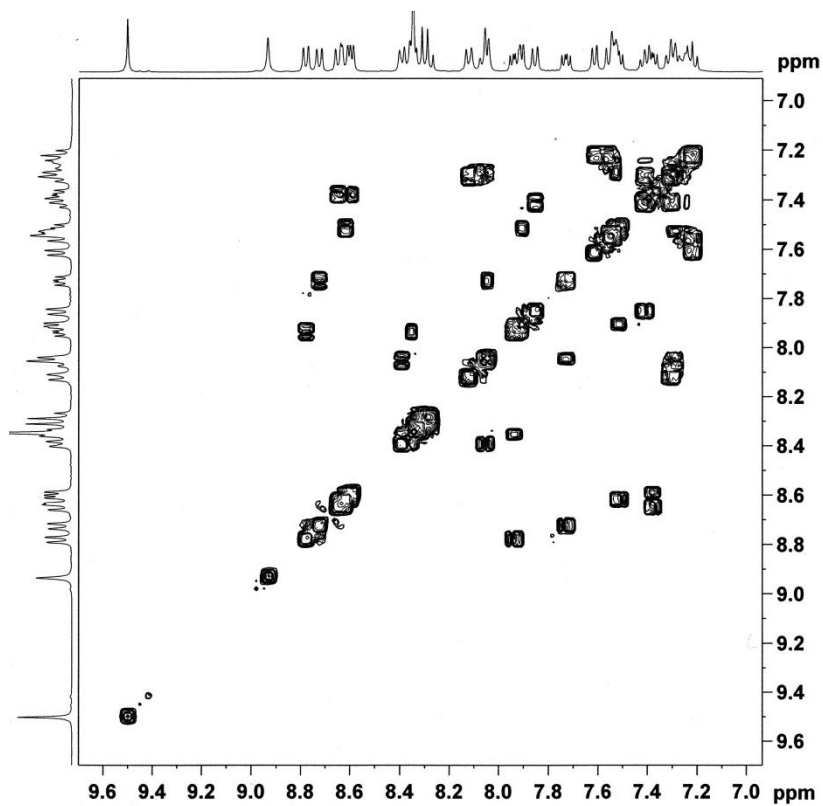


Figure S14. Expanded ^1H - ^1H COSY-NMR of $2[\text{PF}_6]_2$ in $\text{DMSO}-d_6$ at 298K in 500 MHz.

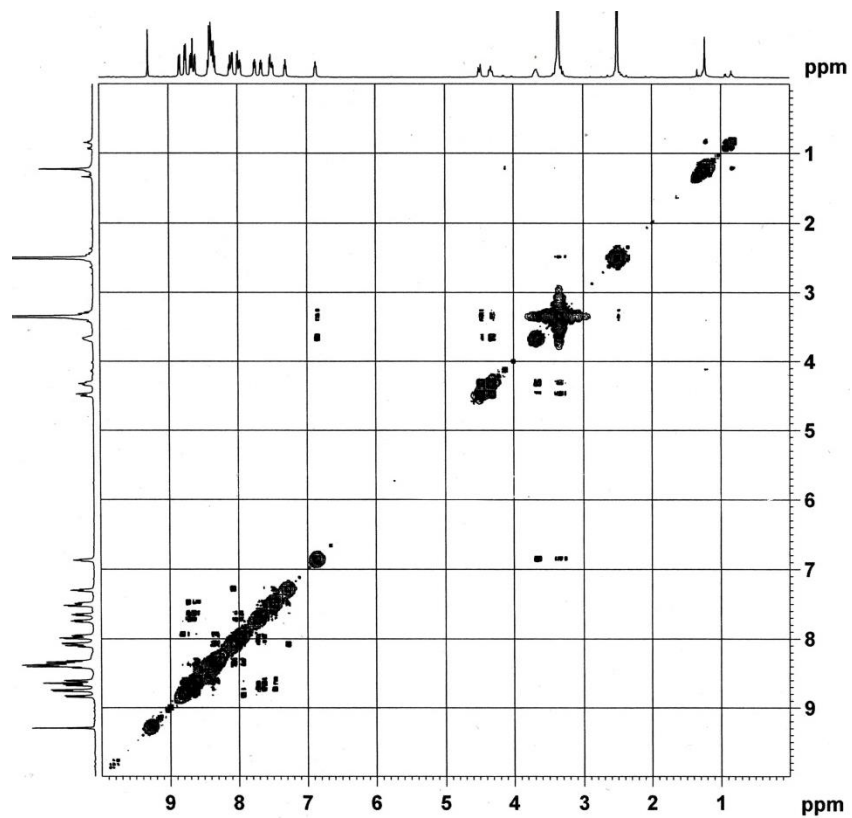


Figure S15. ^1H - ^1H COSY-NMR of complex $2[\text{PF}_6]_2$ in $\text{DMSO-}d_6$ at 298K in 500 MHz.

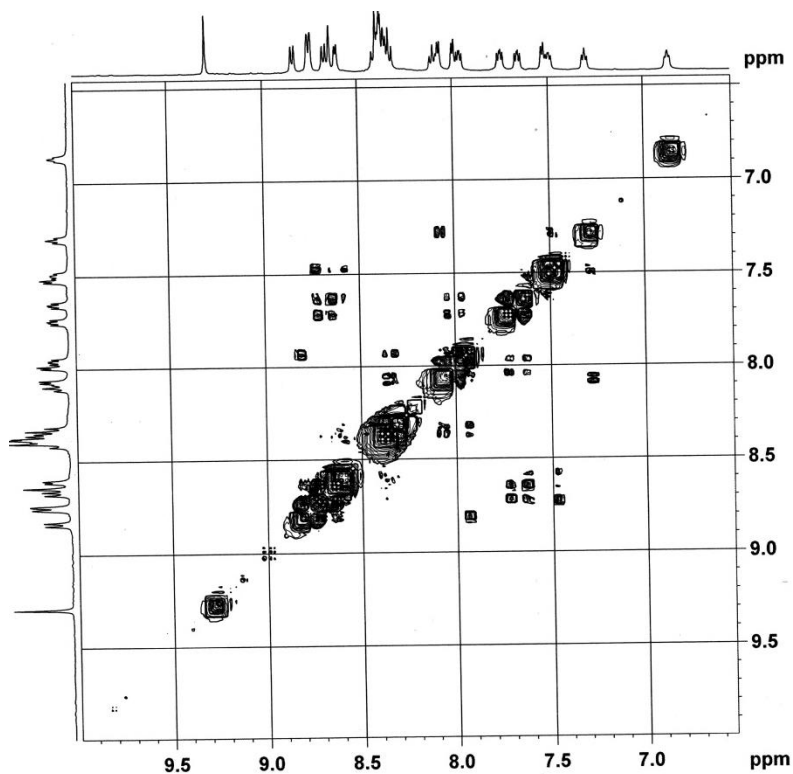


Figure S16. Expanded ^1H - ^1H COSY-NMR of $2[\text{PF}_6]_2$ in $\text{DMSO-}d_6$ at 298K in 500 MHz.

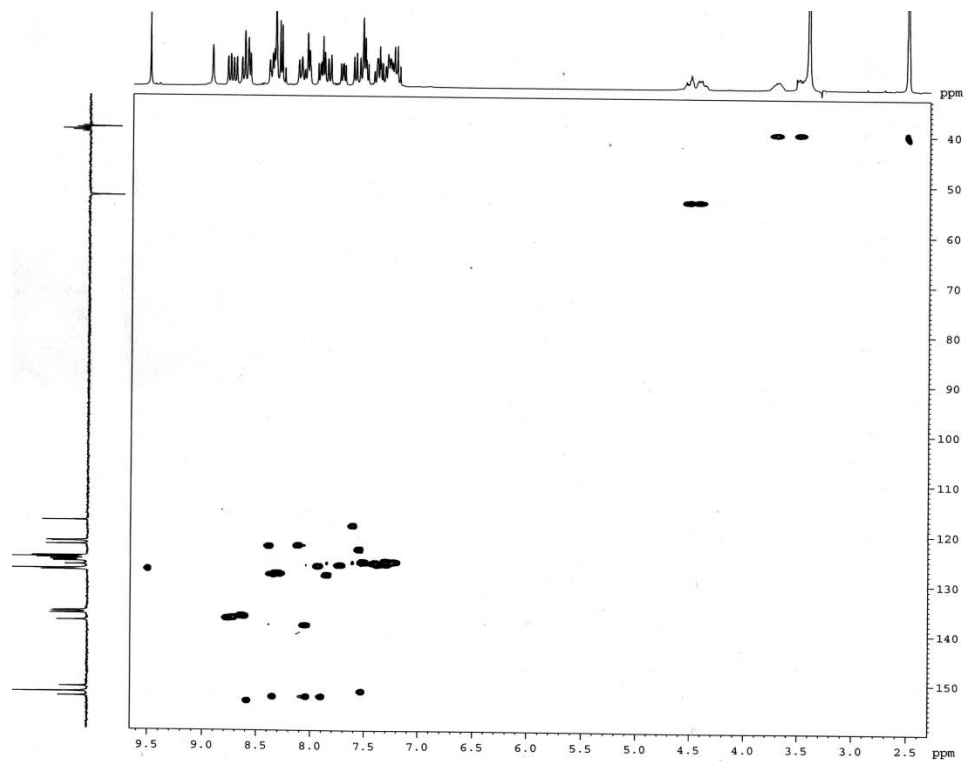


Figure S17. ^1H - ^{13}C HSQC NMR spectrum of $1[\text{PF}_6]_2$ in $\text{DMSO-}d_6$ at 298K in 500 MHz.

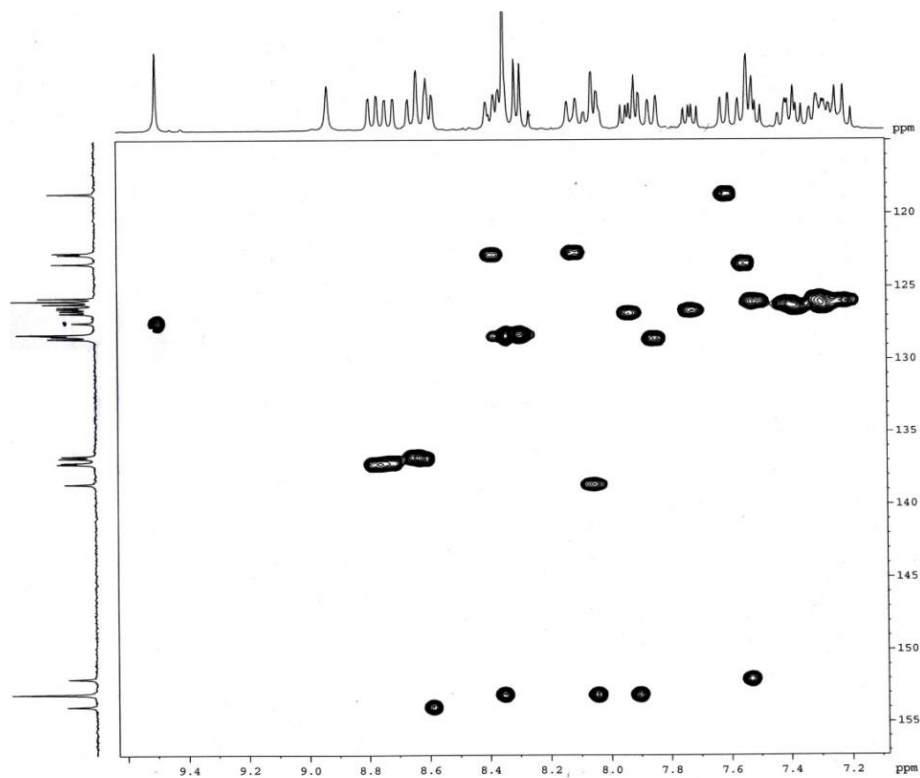


Figure S18. Expanded ^1H - ^{13}C HSQC spectrum of $1[\text{PF}_6]_2$ in $\text{DMSO-}d_6$ at 298K in 500 MHz.

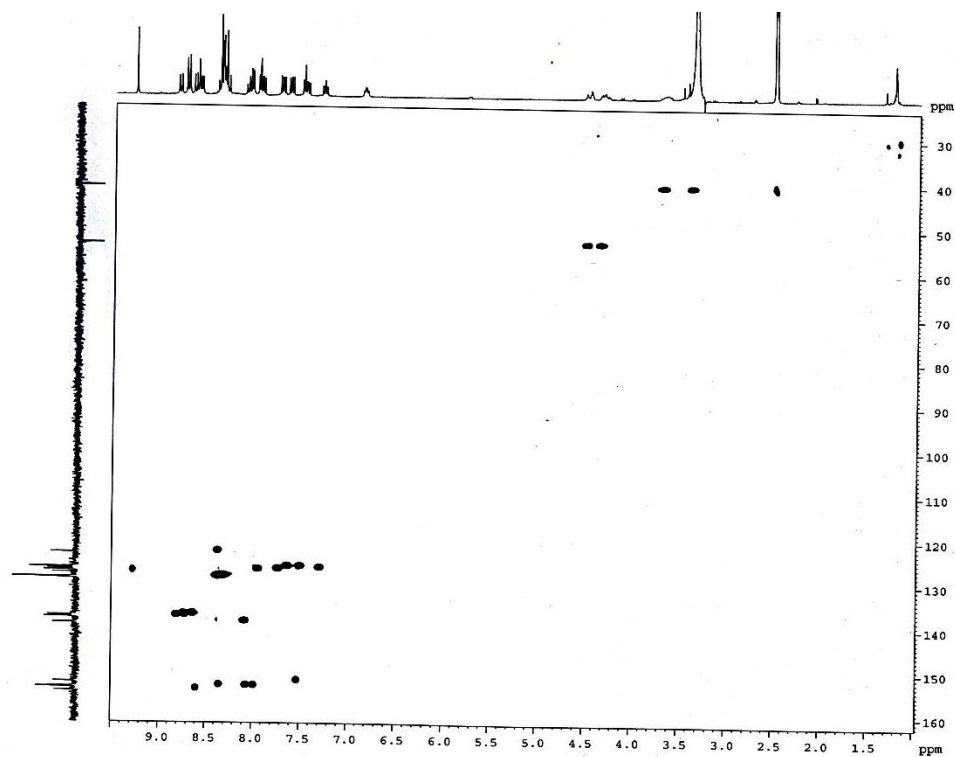


Figure S19. ^1H - ^{13}C HSQC NMR spectrum of $2[\text{PF}_6]_2$ in $\text{DMSO-}d_6$ at 298K in 500 MHz.

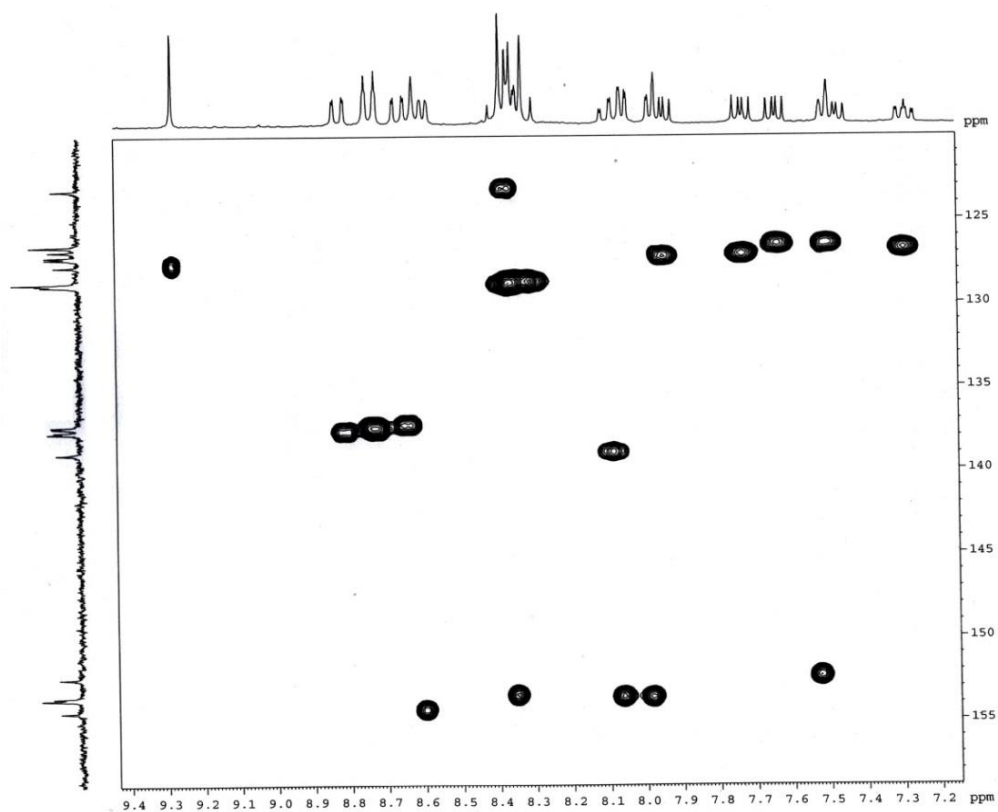


Figure S20. Expanded ^1H - ^{13}C HSQC spectrum of $2[\text{PF}_6]_2$ in $\text{DMSO-}d_6$ at 298K in 500 MHz.

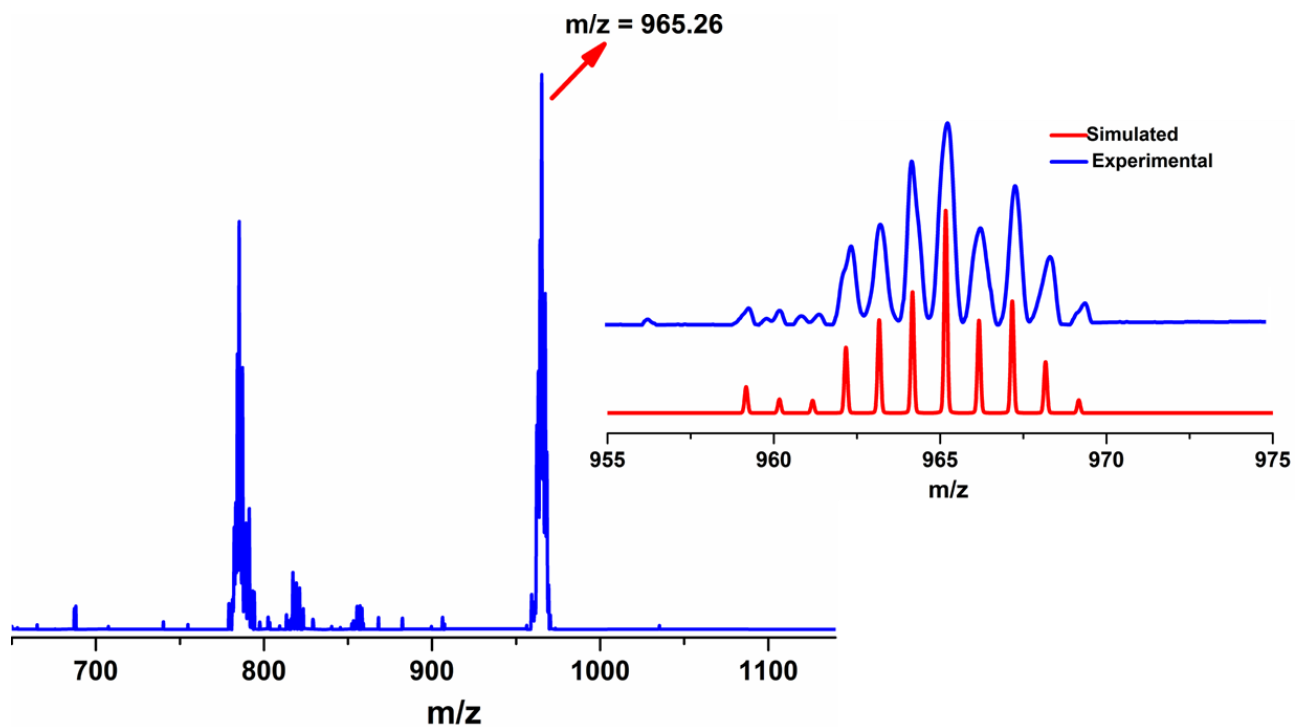


Figure S21. ESI(+Ve) mass spectrum of $1[\text{PF}_6]_2$ with isotopic distribution pattern at 298K.

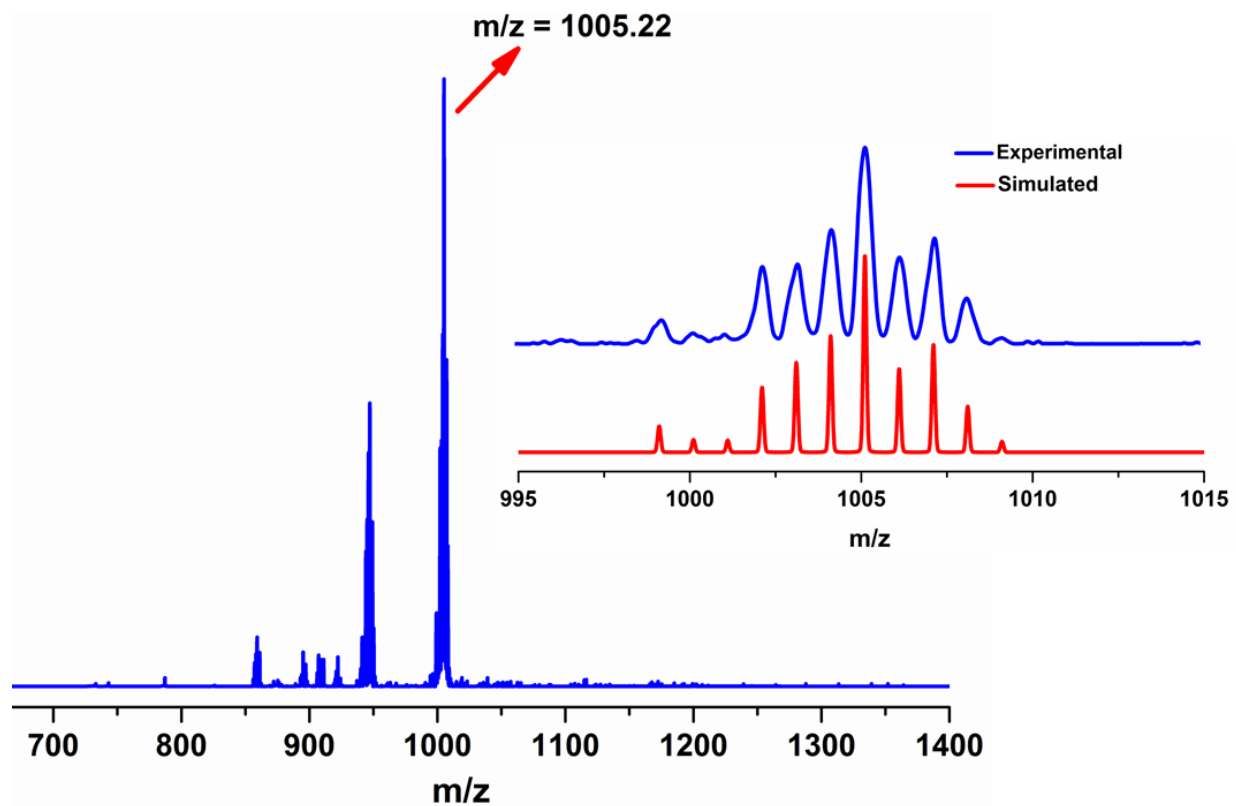


Figure S22. ESI(+Ve) mass spectrum of $2[\text{PF}_6]_2$ with isotopic distribution pattern at 298K.

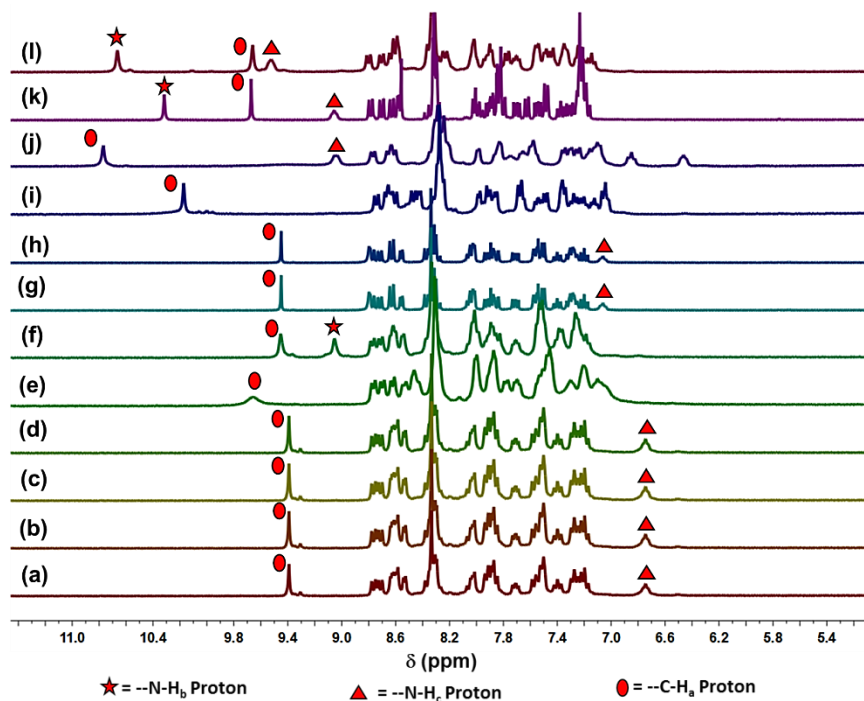


Figure S23. Partial ¹H-NMR spectra of (a) complex **1**[PF₆]₂ (4.7 × 10⁻³ M) and complex **1**[PF₆]₂ with three equivalents of (b) TBANO₃, (c) TBAHSO₄, (d) TBAClO₄, (e) TBAF, (f) TBACl, (g) TBABr, (h) TBAI, (i) (TBA)₃HP₂O₇, (j) TBAH₂PO₄, (k) TBAO₂CPh, (l) TBAO₂CCH₃

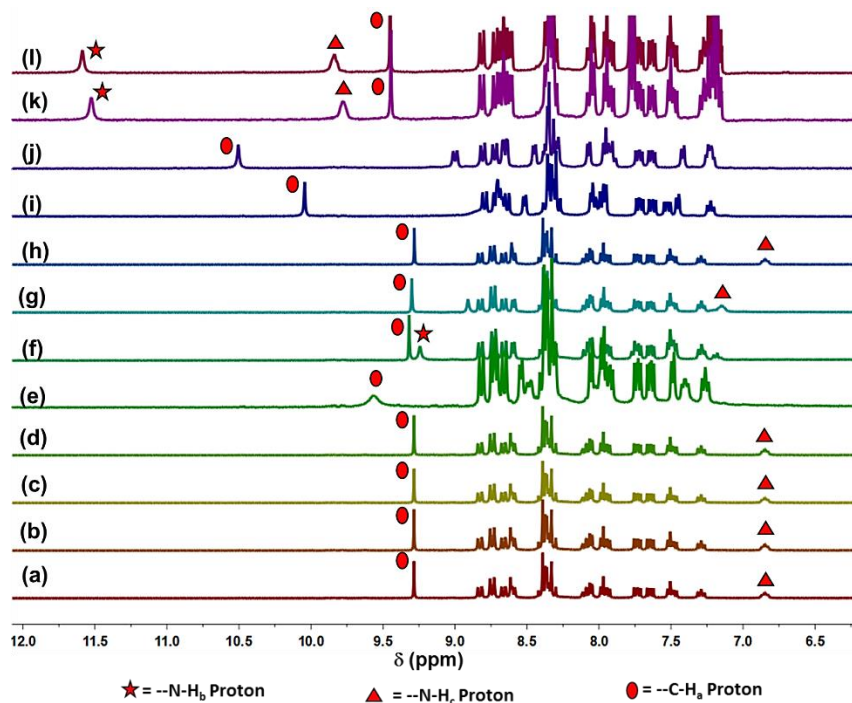


Figure S24. Partial ¹H-NMR spectra of (a) complex **2**[PF₆]₂ (6.2 × 10⁻³ M) and complex **2**[PF₆]₂ with three equivalents of (b) TBANO₃, (c) TBAHSO₄, (d) TBAClO₄, (e) TBAF, (f) TBACl, (g) TBABr, (h) TBAI, (i) (TBA)₃HP₂O₇, (j) TBAH₂PO₄, (k) TBAO₂CPh, (l) TBAO₂CCH₃.

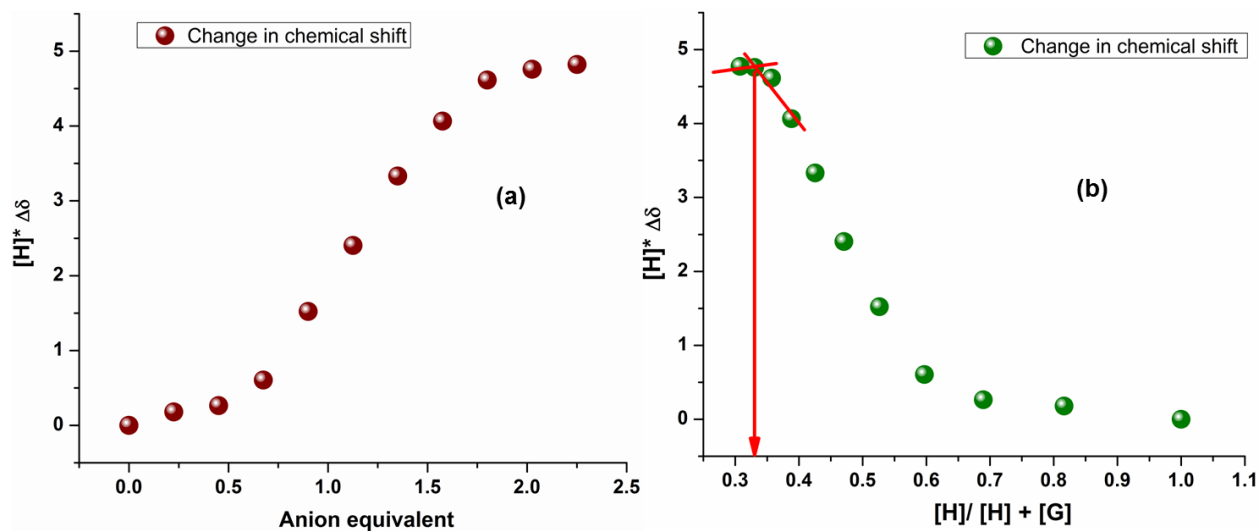


Figure S25. (a) Plot of change in the chemical shift of the triazole $-\text{CH}_a$ groups of complex $1[\text{PF}_6]_2$ (3.2×10^{-3} M) with increasing amounts of TBAH_2PO_4 (4.6×10^{-2} M) in $\text{DMSO}-d_6$ at 298K; (b) Molar ratio plot of titration between complex $1[\text{PF}_6]_2$ with TBAH_2PO_4 obtained by monitoring the shift in resonance position of triazole $-\text{CH}_a$ proton.

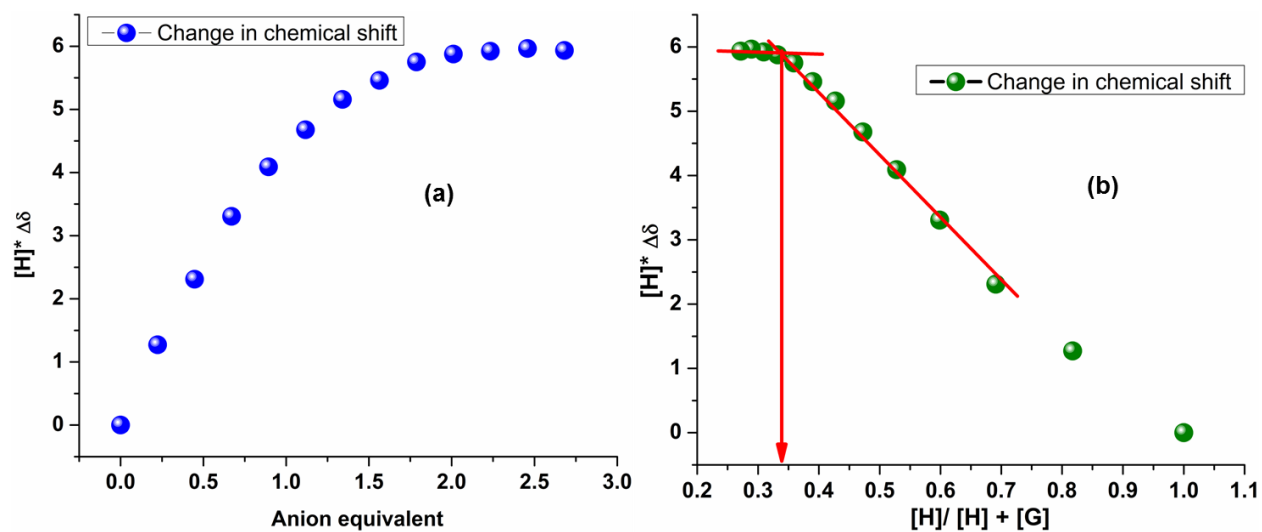


Figure S26. (a) Plot of change in the chemical shift of the triazole $-\text{CH}_a$ groups of complex $2[\text{PF}_6]_2$ (2.7×10^{-3} M) with increasing amounts of TBAH_2PO_4 (3.9×10^{-2} M) in $\text{DMSO}-d_6$ at 298K; (b) Molar ratio plot of titration between complex $2[\text{PF}_6]_2$ with TBAH_2PO_4 obtained by monitoring the shift in resonance position of triazole $-\text{CH}_a$ proton.

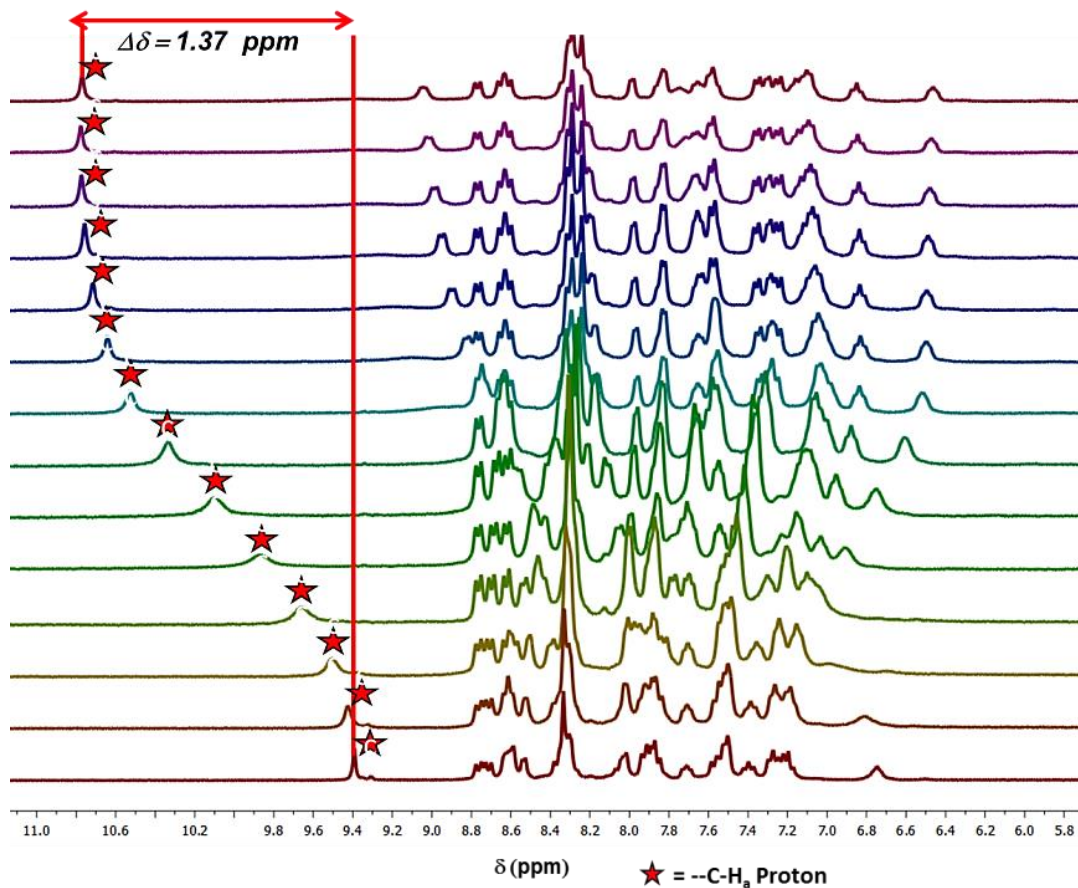


Figure S27. ^1H -NMR titration profile of complex $1[\text{PF}_6]_2$ (1.5×10^{-3} M) with $(\text{TBA})_3\text{HP}_2\text{O}_7$ (2.37×10^{-2} M) in $\text{DMSO}-d_6$.

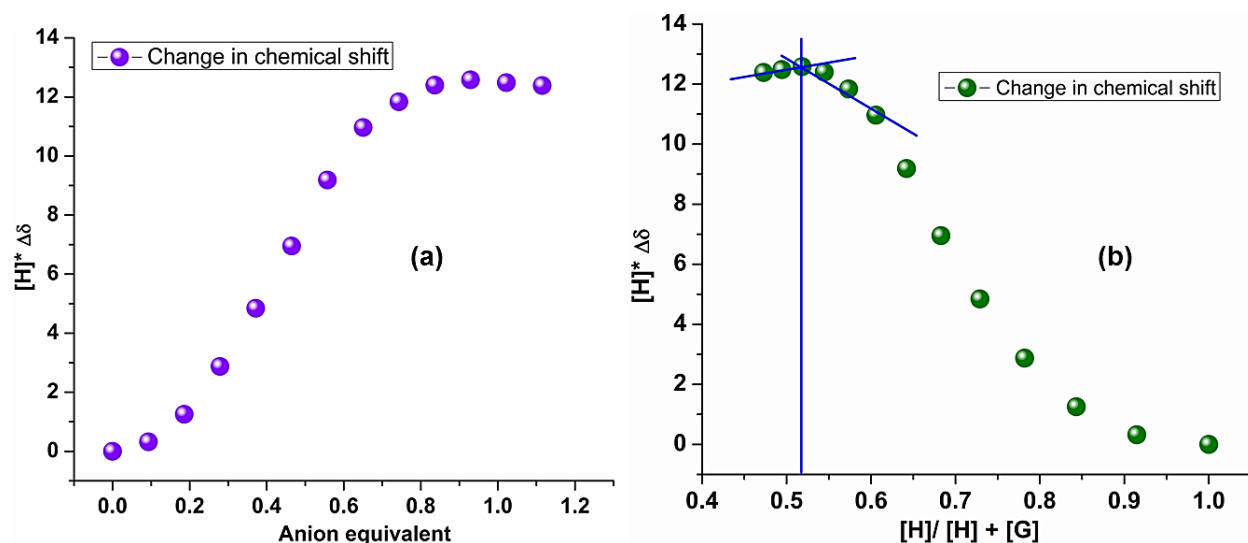


Figure S28. (a) Plot of change in the chemical shift of the triazole $-\text{CH}_a$ groups of complex $1[\text{PF}_6]_2$ (1.5×10^{-3} M) with increasing amounts of $(\text{TBA})_3\text{HP}_2\text{O}_7$ (2.37×10^{-2} M) in $\text{DMSO}-d_6$ at 298K; (b) Molar ratio plot of titration between complex $1[\text{PF}_6]_2$ with $(\text{TBA})_3\text{HP}_2\text{O}_7$ obtained by monitoring the shift in resonance position of triazole $-\text{CH}_a$ proton.

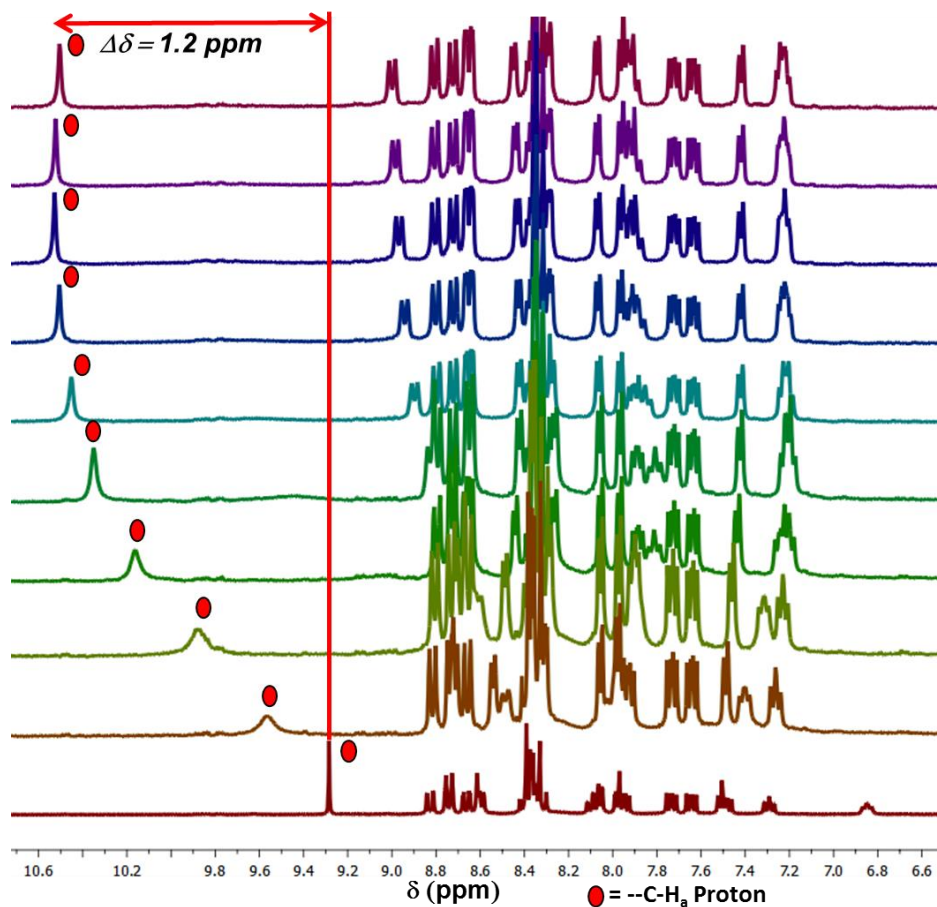


Figure S29. $^1\text{H-NMR}$ titration profile of complex $2[\text{PF}_6]_2$ ($1.67 \times 10^{-3} \text{ M}$) with $(\text{TBA})_3\text{HP}_2\text{O}_7$ ($3.78 \times 10^{-2} \text{ M}$) in $\text{DMSO-}d_6$.

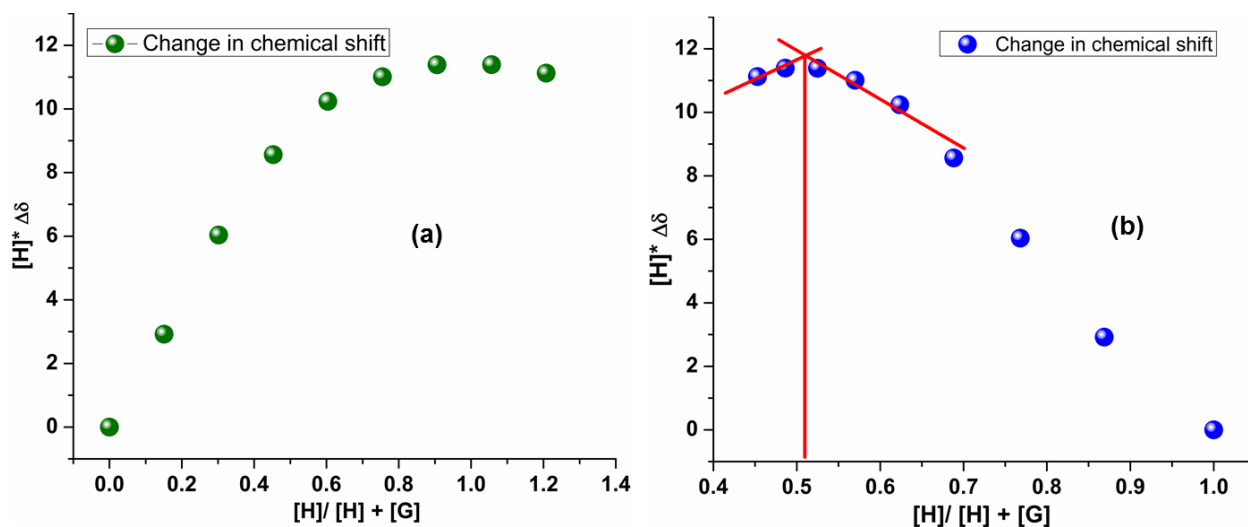


Figure S30. (a) Plot of change in the chemical shift of the triazole $-\text{CH}_a$ groups of complex $2[\text{PF}_6]_2$ ($1.67 \times 10^{-3} \text{ M}$) with increasing amounts of $(\text{TBA})_3\text{HP}_2\text{O}_7$ ($3.78 \times 10^{-2} \text{ M}$) in $\text{DMSO-}d_6$ at 298K; (b) Molar ratio plot of titration between complex $2[\text{PF}_6]_2$ with $(\text{TBA})_3\text{HP}_2\text{O}_7$ obtained by monitoring the shift in resonance position of triazole $-\text{CH}_a$ proton.

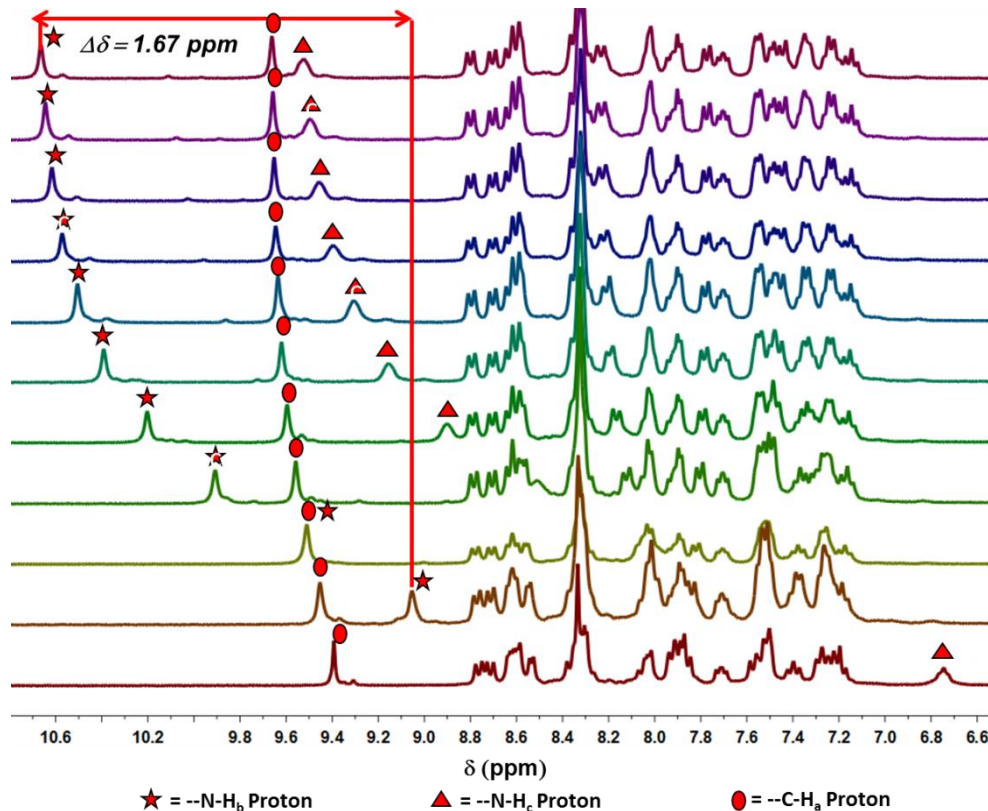


Figure S31. $^1\text{H-NMR}$ titration profile of complex $1[\text{PF}_6]_2$ ($4.28 \times 10^{-3} \text{ M}$) with $\text{TBAO}_2\text{CCH}_3$ ($9.12 \times 10^{-2} \text{ M}$) in $\text{DMSO-}d_6$.

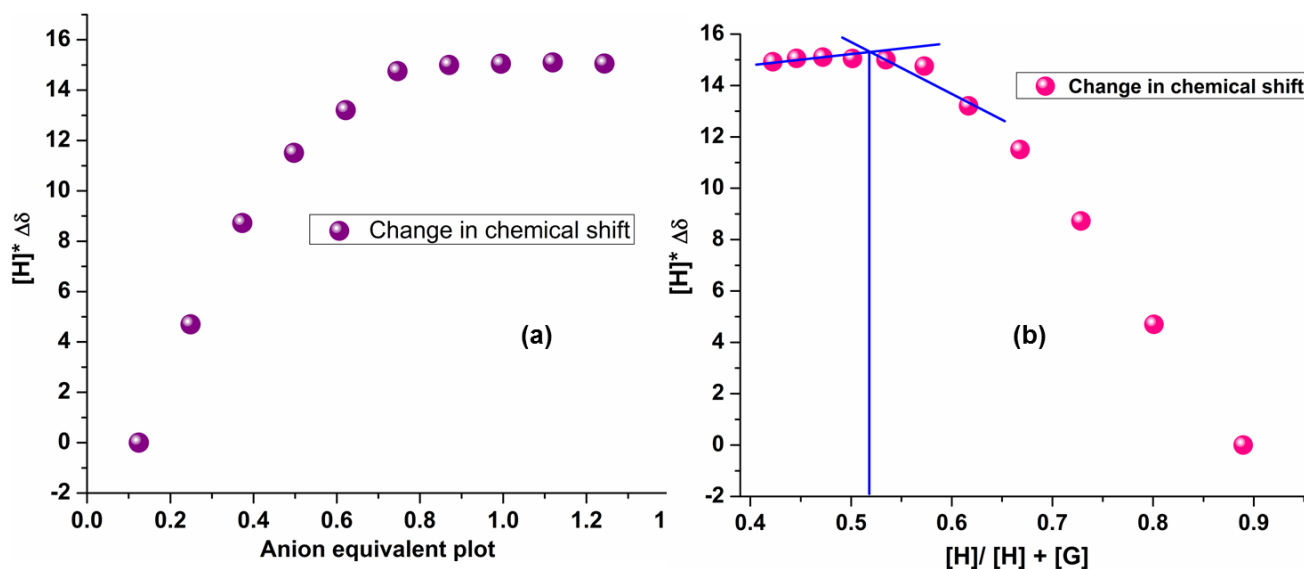


Figure S32. (a) Plot of change in the chemical shift of the triazole $-\text{CH}_a$ groups of complex $1[\text{PF}_6]_2$ ($4.28 \times 10^{-3} \text{ M}$) with increasing amounts of $\text{TBAO}_2\text{CCH}_3$ ($9.12 \times 10^{-2} \text{ M}$) in $\text{DMSO-}d_6$ at 298K; (b) Molar ratio plot of titration between complex $1[\text{PF}_6]_2$ with $\text{TBAO}_2\text{CCH}_3$ obtained by monitoring the shift in resonance position of triazole $-\text{CH}_a$ proton.

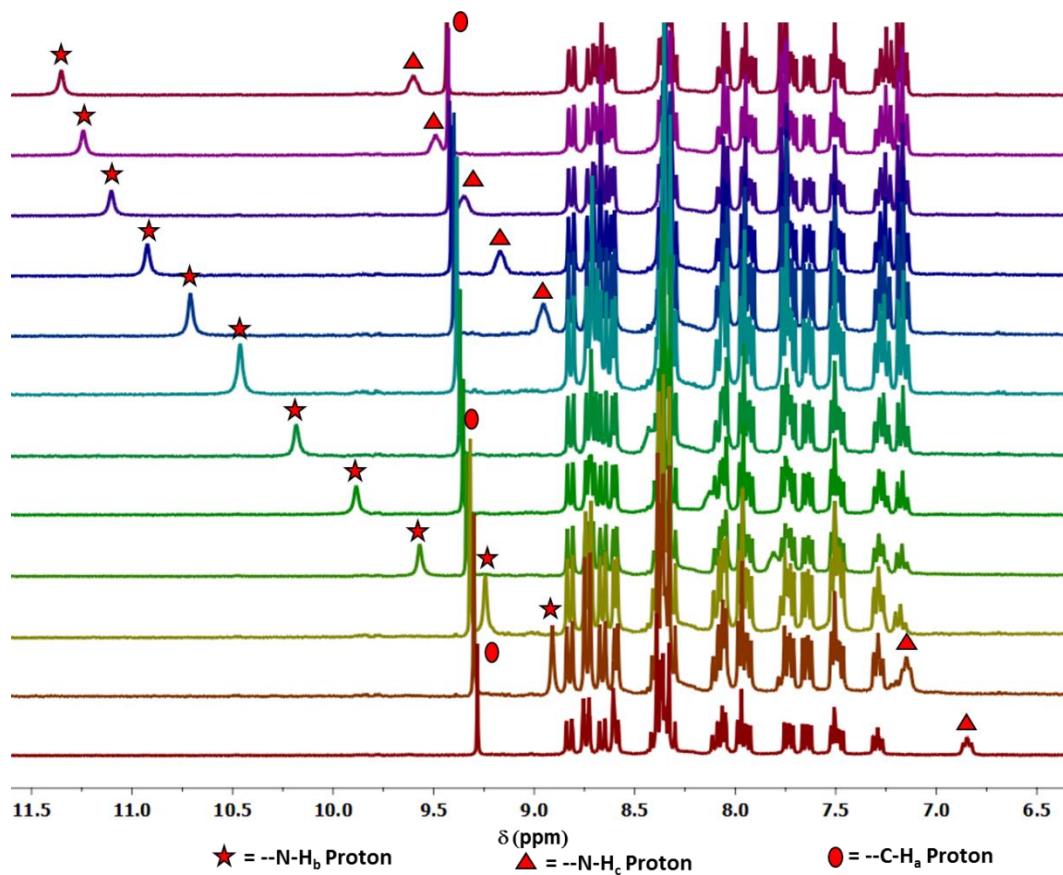


Figure S33. $^1\text{H-NMR}$ titration profile of complex $2[\text{PF}_6]_2$ ($4.56 \times 10^{-3} \text{ M}$) with $\text{TBAO}_2\text{CCH}_3$ ($9.68 \times 10^{-2} \text{ M}$) in $\text{DMSO-}d_6$.

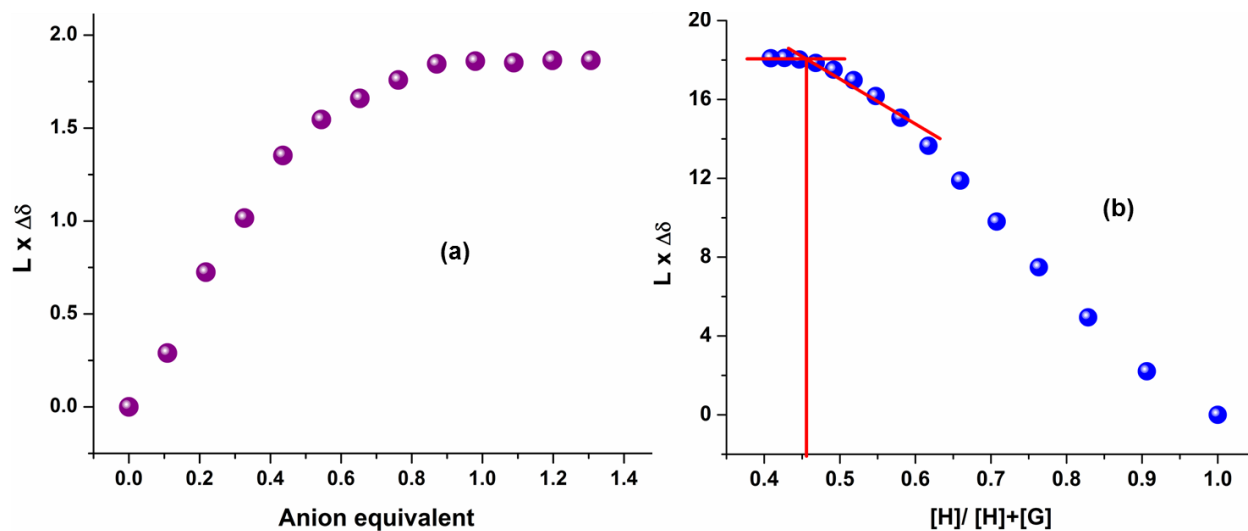


Figure S34. (a) Plot of change in the chemical shift of the triazole $-\text{CH}_a$ groups of complex $2[\text{PF}_6]_2$ ($4.56 \times 10^{-3} \text{ M}$) with increasing amounts of $\text{TBAO}_2\text{CCH}_3$ ($9.68 \times 10^{-2} \text{ M}$) in $\text{DMSO-}d_6$ at 298K ; (b) Molar ratio plot of titration between complex $2[\text{PF}_6]_2$ with $\text{TBAO}_2\text{CCH}_3$ obtained by monitoring the shift in resonance position of triazole $-\text{CH}_a$ proton.

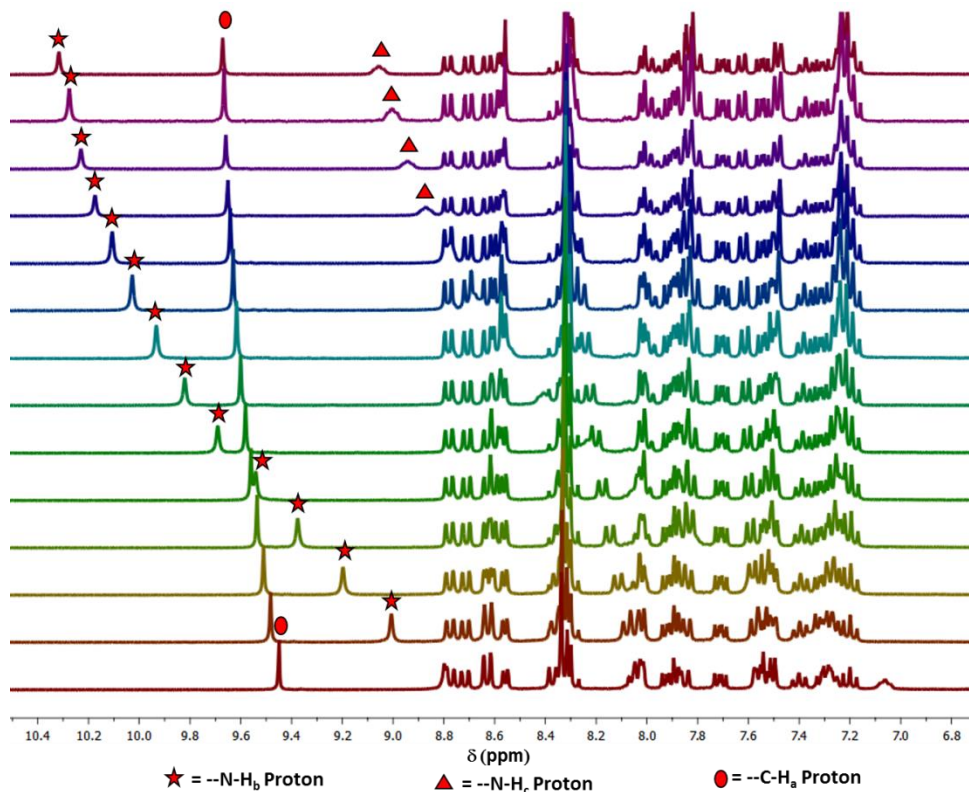


Figure S35. ^1H -NMR titration profile of complex $1[\text{PF}_6]_2$ ($3.61 \times 10^{-3} \text{ M}$) with TBAO_2CPh ($6.59 \times 10^{-2} \text{ M}$) in $\text{DMSO}-d_6$.

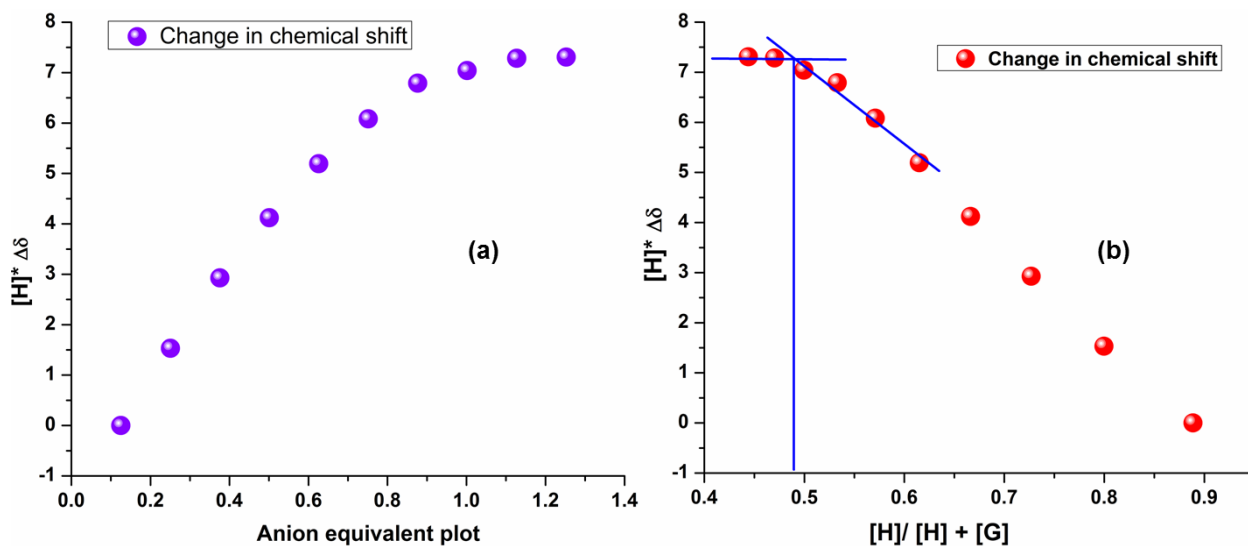


Figure S36. (a) Plot of change in the chemical shift of the triazole $-\text{CH}_a$ groups of complex $1[\text{PF}_6]_2$ ($3.61 \times 10^{-3} \text{ M}$) with increasing amounts of TBAO_2CPh ($6.59 \times 10^{-2} \text{ M}$) in $\text{DMSO}-d_6$ at 298K; (b) Molar ratio plot of titration between complex $1[\text{PF}_6]_2$ with TBAO_2CPh obtained by monitoring the shift in resonance position of triazole $-\text{CH}_a$ proton.

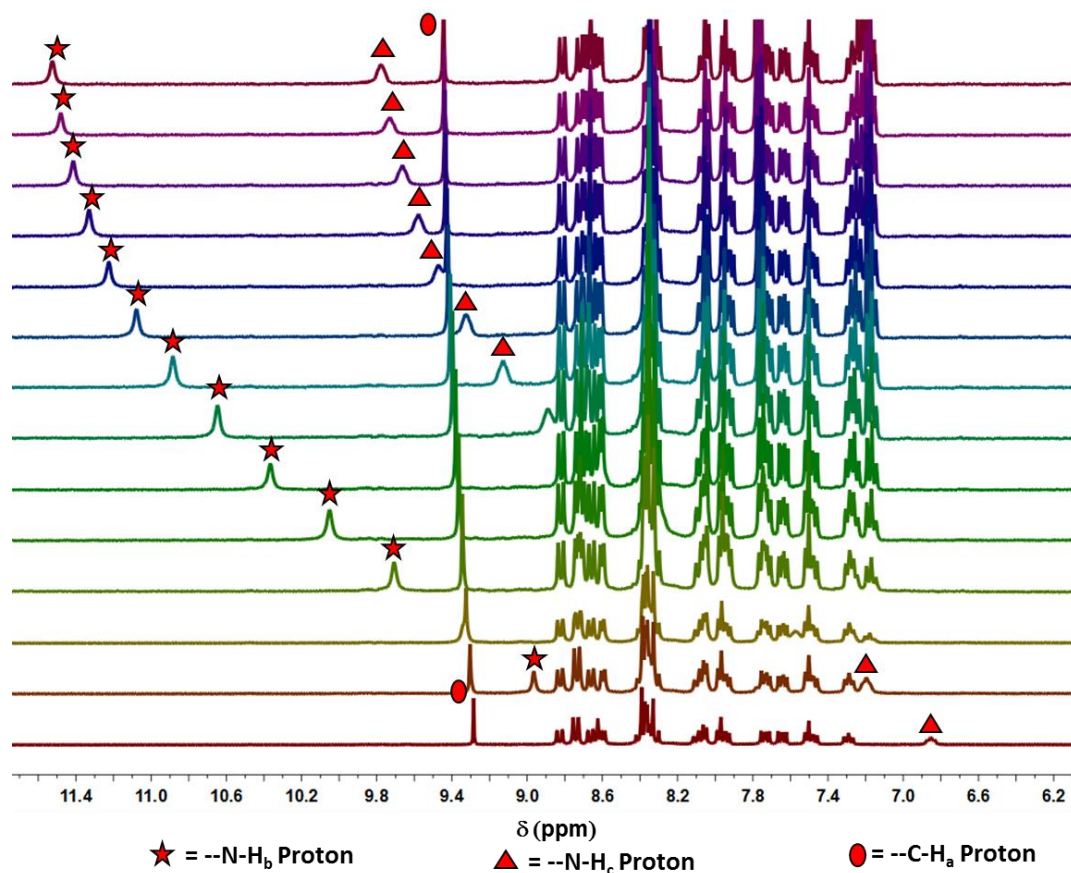


Figure S37. $^1\text{H-NMR}$ titration profile of complex $2[\text{PF}_6]_2$ ($4.06 \times 10^{-3} \text{ M}$) with TBAO_2CPh ($7.49 \times 10^{-2} \text{ M}$) in $\text{DMSO-}d_6$.

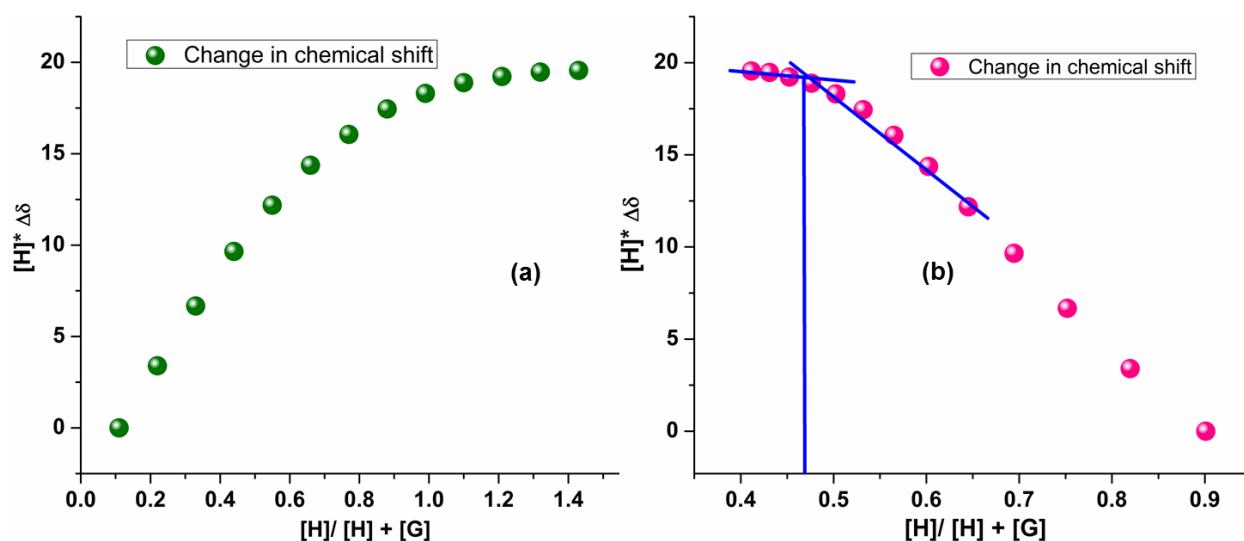


Figure S38. (a) Plot of change in the chemical shift of the triazole $-\text{CH}_a$ groups of complex $2[\text{PF}_6]_2$ ($4.06 \times 10^{-3} \text{ M}$) with increasing amounts of TBAO_2CPh ($7.49 \times 10^{-2} \text{ M}$) in $\text{DMSO-}d_6$ at 298K; (b) Molar ratio plot of titration between complex $2[\text{PF}_6]_2$ with TBAO_2CPh obtained by monitoring the shift in resonance position of triazole $-\text{CH}_a$ proton.

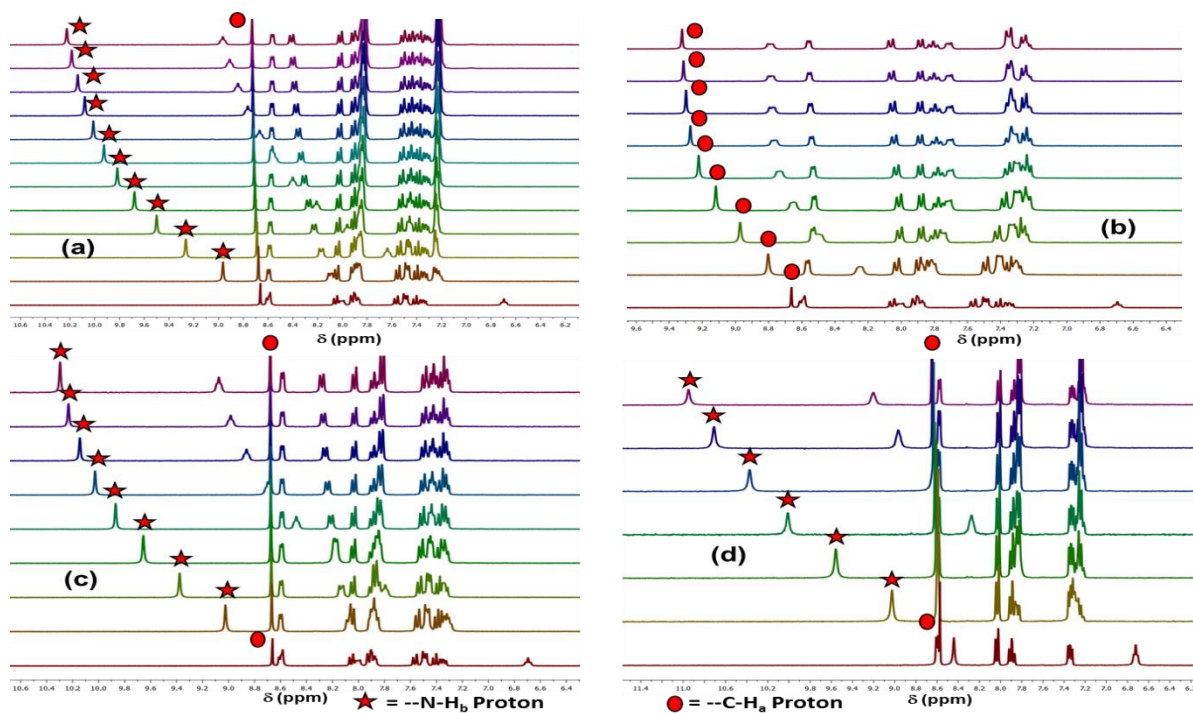


Figure SS38: $^1\text{H-NMR}$ titration profile of (a) **L1** (5.16×10^{-3} M) with TBAH_2PO_4 (8.14×10^{-2} M) (b) **L1** (4.29×10^{-3} M) with $(\text{TBA})_3\text{HP}_2\text{O}_7$ (7.29×10^{-2} M) (c) **L1** (6.24×10^{-3} M) with TBAOAc (9.18×10^{-2} M) (d) **L1** (6.51×10^{-3} M) with TBAO_2CPh (7.58×10^{-2} M) in $\text{DMSO-}d_6$.

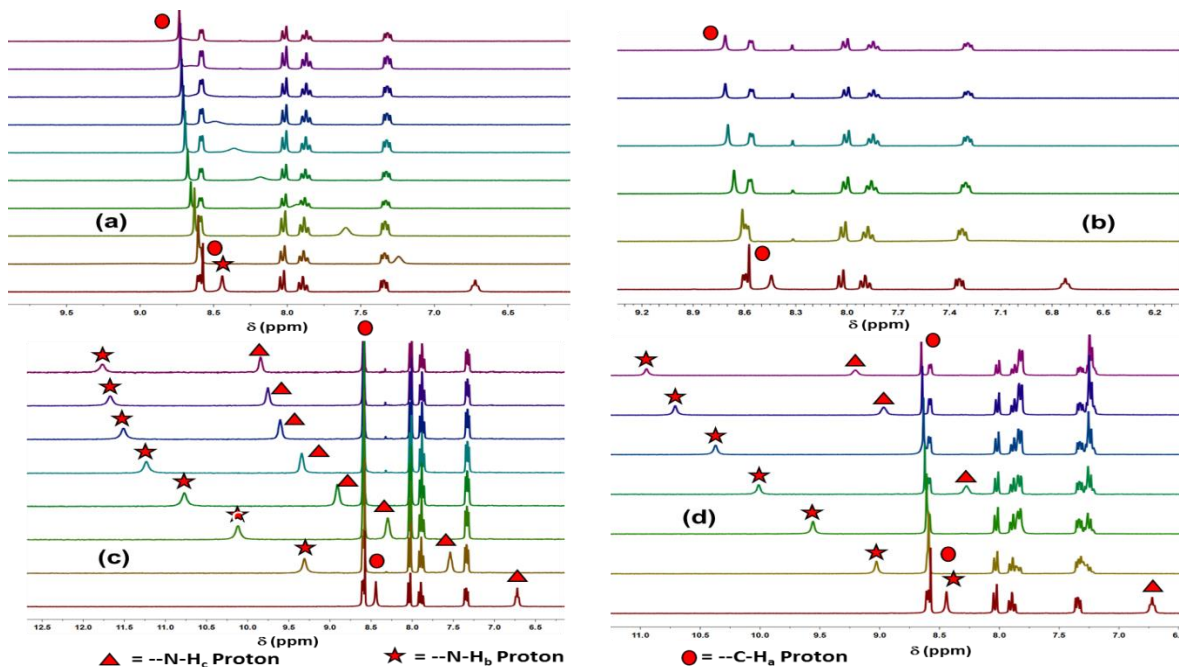


Figure SSS38: $^1\text{H-NMR}$ titration profile of (a) **L2** (5.98×10^{-3} M) with TBAH_2PO_4 (8.89×10^{-2} M) (b) **L2** (5.38×10^{-3} M) with $(\text{TBA})_3\text{HP}_2\text{O}_7$ (9.29×10^{-2} M) (c) **L2** (7.38×10^{-3} M) with TBAOAc (8.63×10^{-2} M) (d) **L2** (4.53×10^{-3} M) with TBAO_2CPh (8.67×10^{-2} M) in $\text{DMSO-}d_6$.

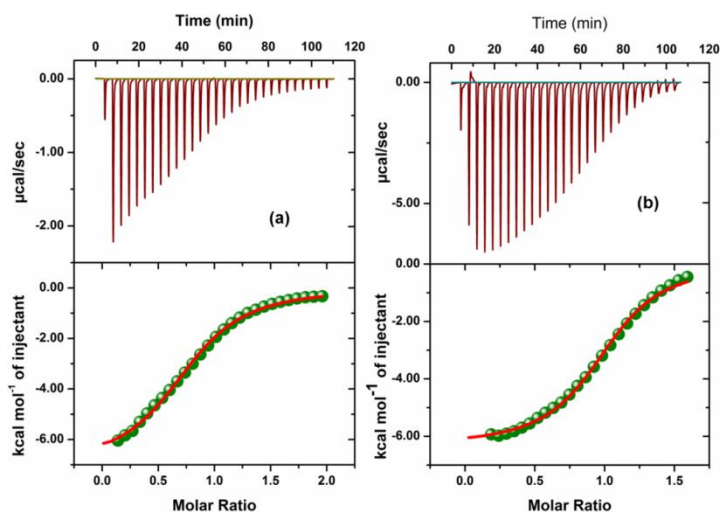


Figure S39. Isothermal titration calorimetric plot at 298 K for the addition of (a) $(\text{TBA})_2\text{HP}_2\text{O}_7$ (0.35 mM) to a solution of $1[\text{PF}_6]_2$ (0.032 mM) in CH_3CN ; (b) $(\text{TBA})_2\text{HP}_2\text{O}_7$ (0.42 mM) to a solution of $2[\text{PF}_6]_2$ (0.6 mM) in CH_3CN . In all the graphs the upper panel shows the heat pulses experimentally observed in each titration. The lower panel reports the respective time integrals translating as the heat evolved for each aliquot and its coherence to one-site binding model.

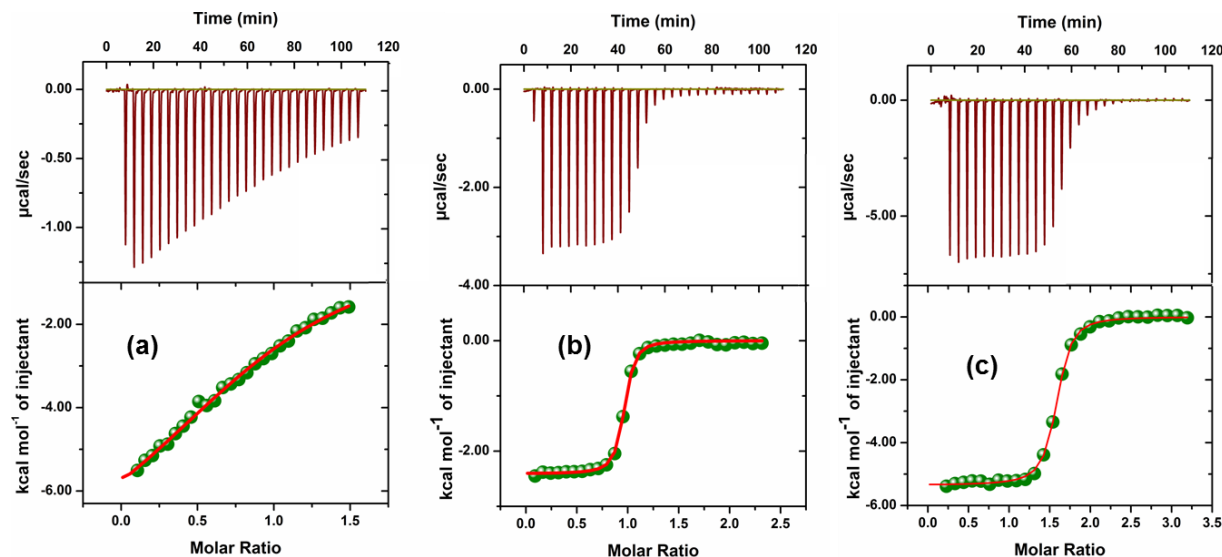


Figure S40. Isothermal titration calorimetric plot at 298 K for the addition of (a) TBAO_2CPh (2.22 mM) to a solution of $2[\text{PF}_6]_2$ (0.32 mM) in CH_3CN ; (b) TBAO_2CPh (6.4 mM) to a solution of $2\text{PF}_6]_2$ (0.6 mM) in CH_3CN ; (c) $\text{TBAO}_2\text{CCH}_3$ (4.52 mM) to a solution of $1[\text{PF}_6]_2$ (0.32 mM) in CH_3CN . In all the graphs the upper panel shows the heat pulses experimentally observed in each titration. The lower panel reports the respective time integrals translating as the heat evolved for each aliquot and its coherence to one-site binding model.

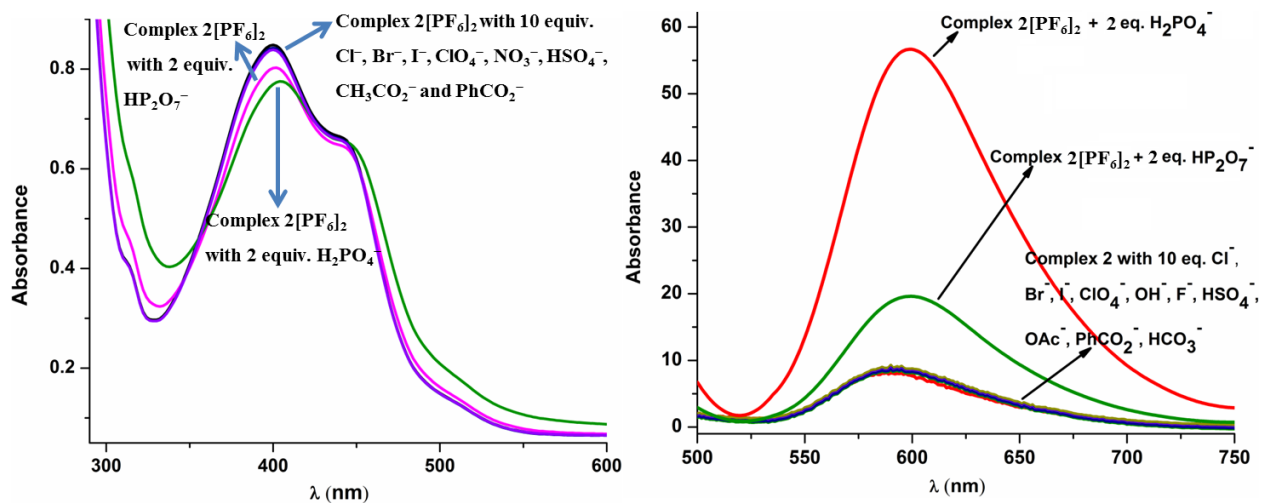


Figure S41. (a) Comparative UV-Visible spectra of complex $2[\text{PF}_6]_2$ ($50\mu\text{M}$) in the presence of 2 equiv. of phosphates (H_2PO_4^- , $\text{HP}_2\text{O}_7^{3-}$) and 10 equiv. of other anions (F^- , Cl^- , Br^- , I^- , ClO_4^- , NO_3^- , HSO_4^- , HCO_3^- , CH_3CO_2^- and PhCO_2^-) in CH_3CN at 298K; (b) PL spectra of complex $2[\text{PF}_6]_2$ ($6\mu\text{M}$) in presence of 10 equivalent of F^- , Cl^- , Br^- , I^- , ClO_4^- , NO_3^- , HSO_4^- , HCO_3^- , CH_3CO_2^- , PhCO_2^- and 2 equivalents of H_2PO_4^- , $\text{HP}_2\text{O}_7^{3-}$ in CH_3CN at 298K.

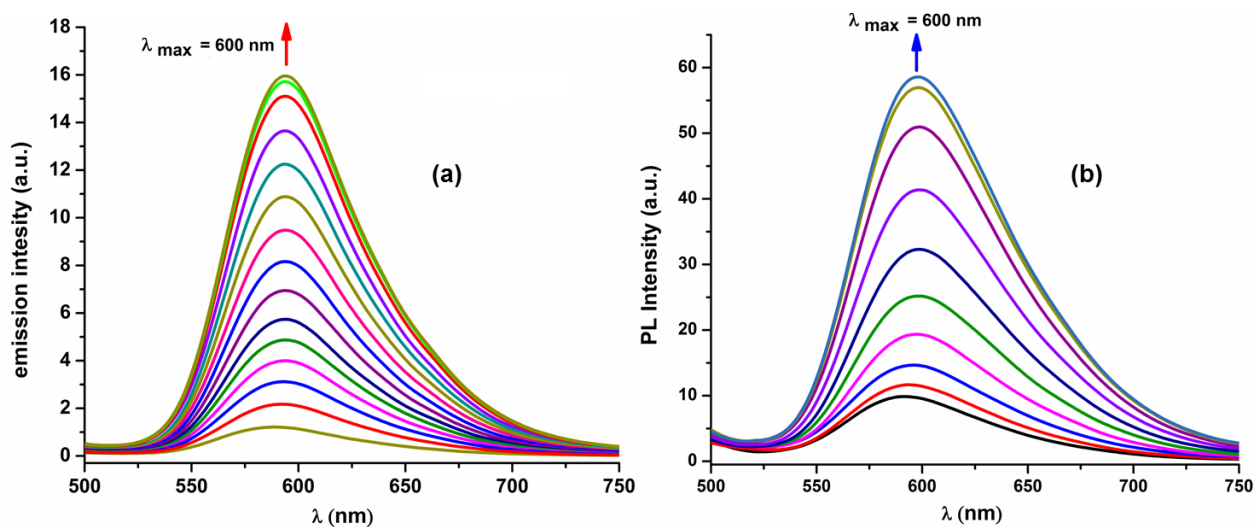


Figure S42. PL titration profile of (a) complex $1[\text{PF}_6]_2$ (6×10^{-6} M) upon addition of (0-2.5 equiv.) of H_2PO_4^- (3×10^{-4} M) in CH_3CN and (b) complex $2[\text{PF}_6]_2$ (6×10^{-6} M) upon addition of (0-2.3 equiv.) of H_2PO_4^- (3×10^{-4} M) in CH_3CN at 298K.

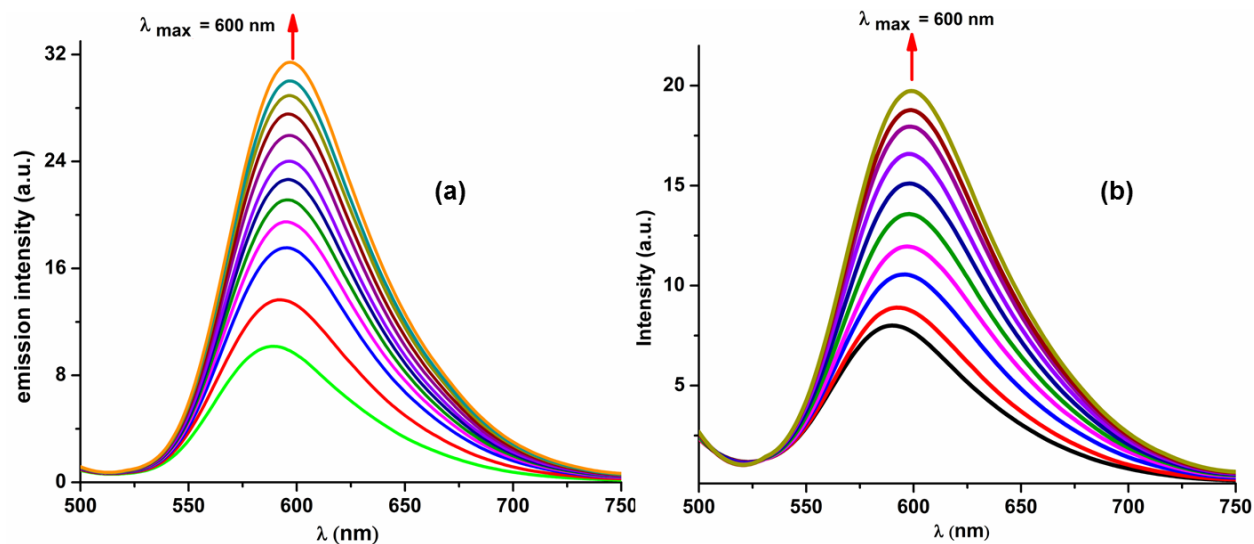


Figure S43. PL titration profile of (a) complex $1[\text{PF}_6]_2$ (6×10^{-6} M) upon addition of (0-1.3 equiv.) of $\text{HP}_2\text{O}_7^{3-}$ (1.5×10^{-4} M) in CH_3CN at 298K; (b) complex $2[\text{PF}_6]_2$ (6×10^{-6} M) upon addition of (0-1.3 equiv.) of $\text{HP}_2\text{O}_7^{3-}$ (1.5×10^{-4} M) in CH_3CN at 298K.

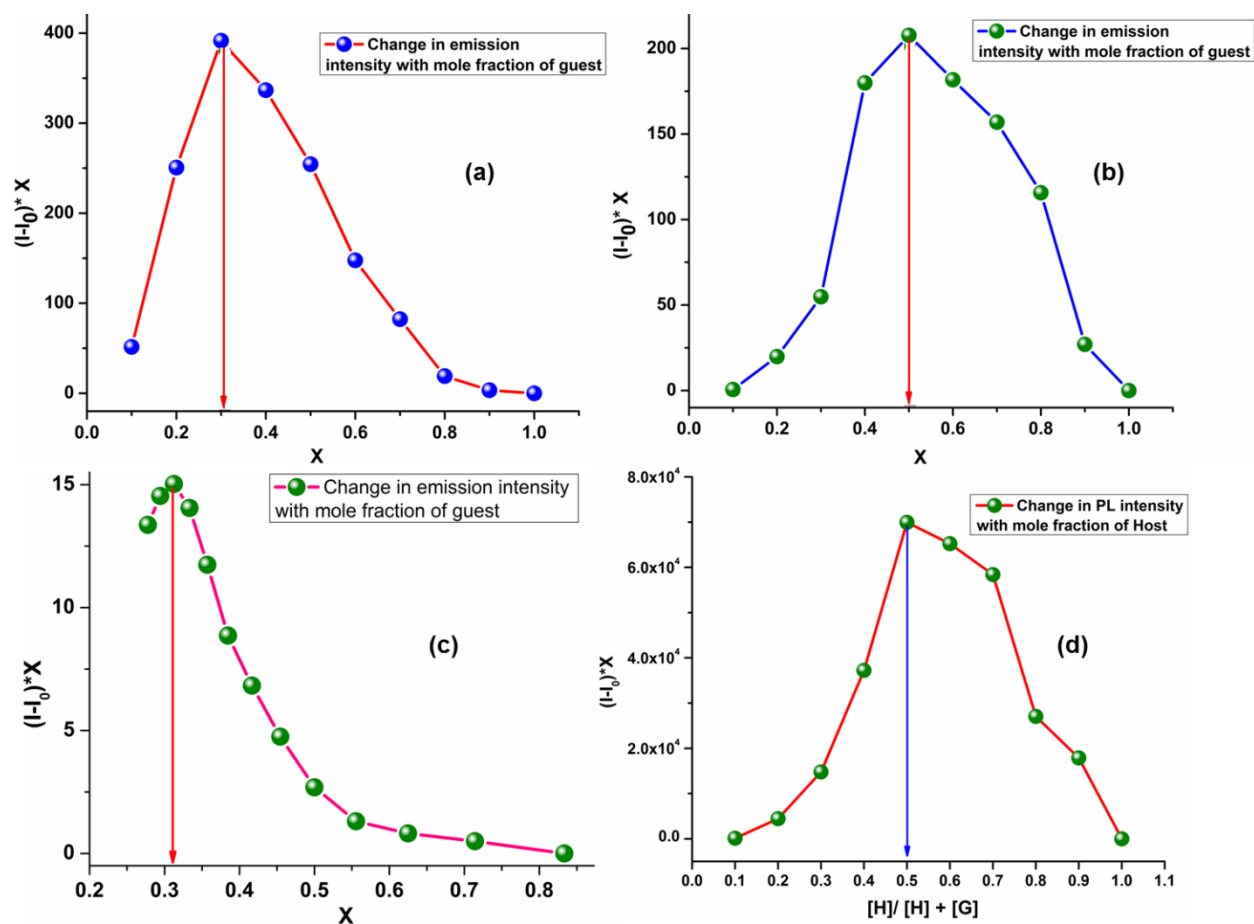


Figure S44. Molar ratio plot from PL titration in CH_3CN between (a) $1[\text{PF}_6]_2$ and H_2PO_4^- (b) $1[\text{PF}_6]_2$ and $\text{HP}_2\text{O}_7^{3-}$ (c) $2[\text{PF}_6]_2$ and H_2PO_4^- (d) $2[\text{PF}_6]_2$ and $\text{HP}_2\text{O}_7^{3-}$.

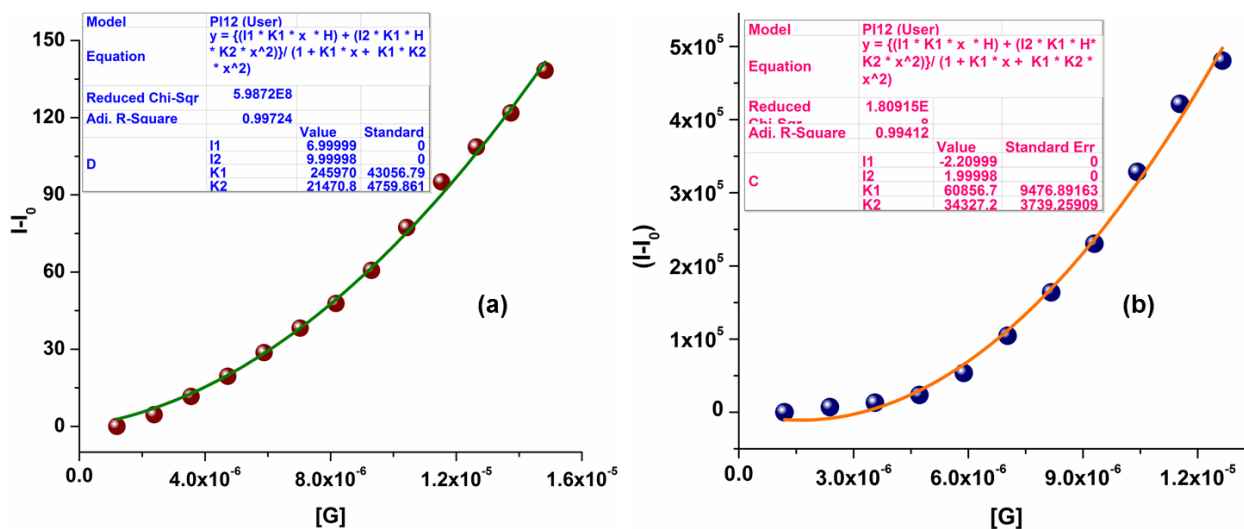


Figure S45. Non-linear 1:2 curve fitting of PL titration data in CH₃CN at 298K to calculate association constant of (a) **1[PF₆]₂** with TBAH₂PO₄ and (b) **2[PF₆]₂** with TBAH₂PO₄.

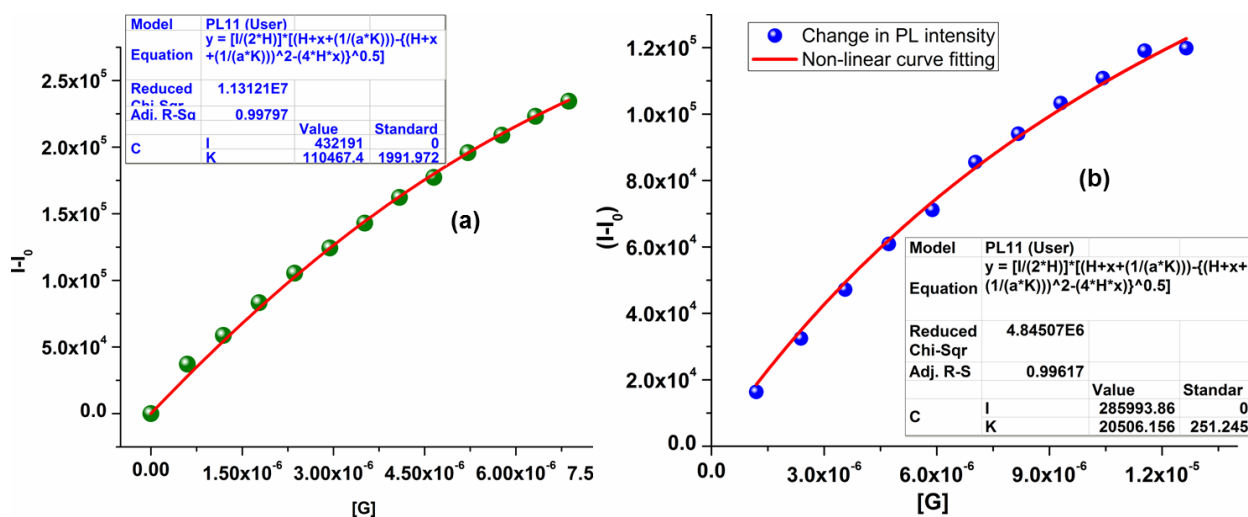


Figure S46. Non-linear 1:1 curve fitting of PL titration data in CH₃CN at 298K to calculate association constant of (a) **1[PF₆]₂** with (TBA)₃HP₂O₇ and (b) **2[PF₆]₂** with (TBA)₃HP₂O₇.

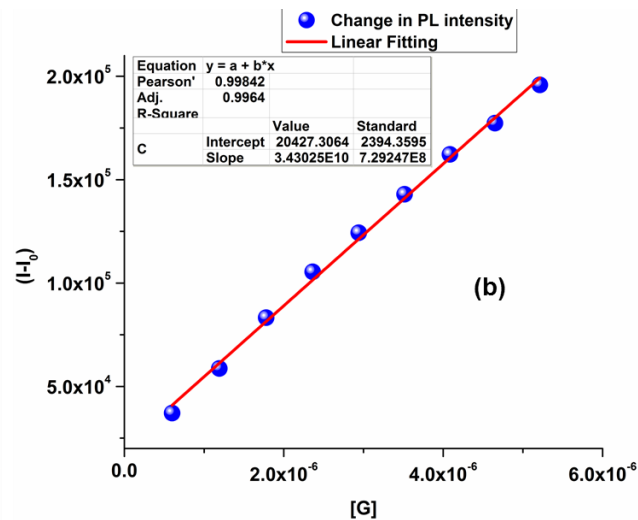
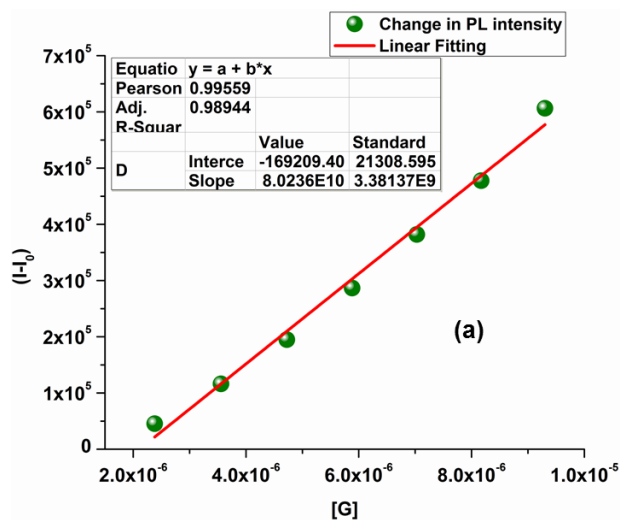


Figure S47. Calibration curve from PL titration for $1[\text{PF}_6]_2$ ($10.0 \mu\text{M}$) with (a) H_2PO_4^- over the concentration range between 2.0 and $10.0 \mu\text{M}$ (b) $\text{HP}_2\text{O}_7^{3-}$ over the concentration range between 0 and $6.0 \mu\text{M}$.

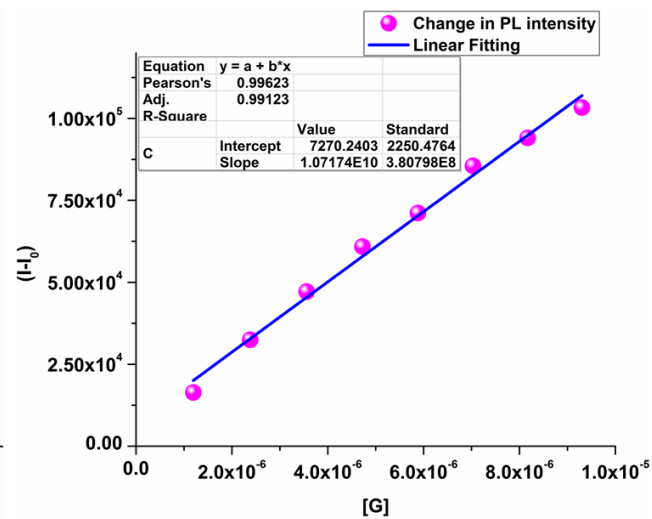
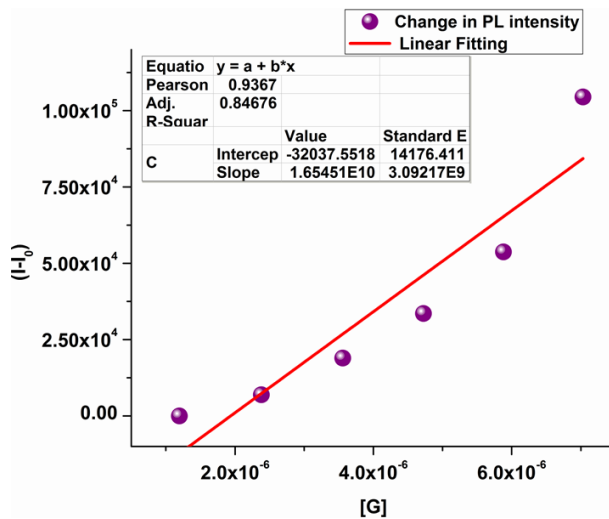


Figure S48. Calibration curve from PL titration for $2[\text{PF}_6]_2$ ($10.0 \mu\text{M}$) with (a) H_2PO_4^- over the concentration range between 1.0 and $8.0 \mu\text{M}$ (b) $\text{HP}_2\text{O}_7^{3-}$ over the concentration range between 1.0 and $10.0 \mu\text{M}$.

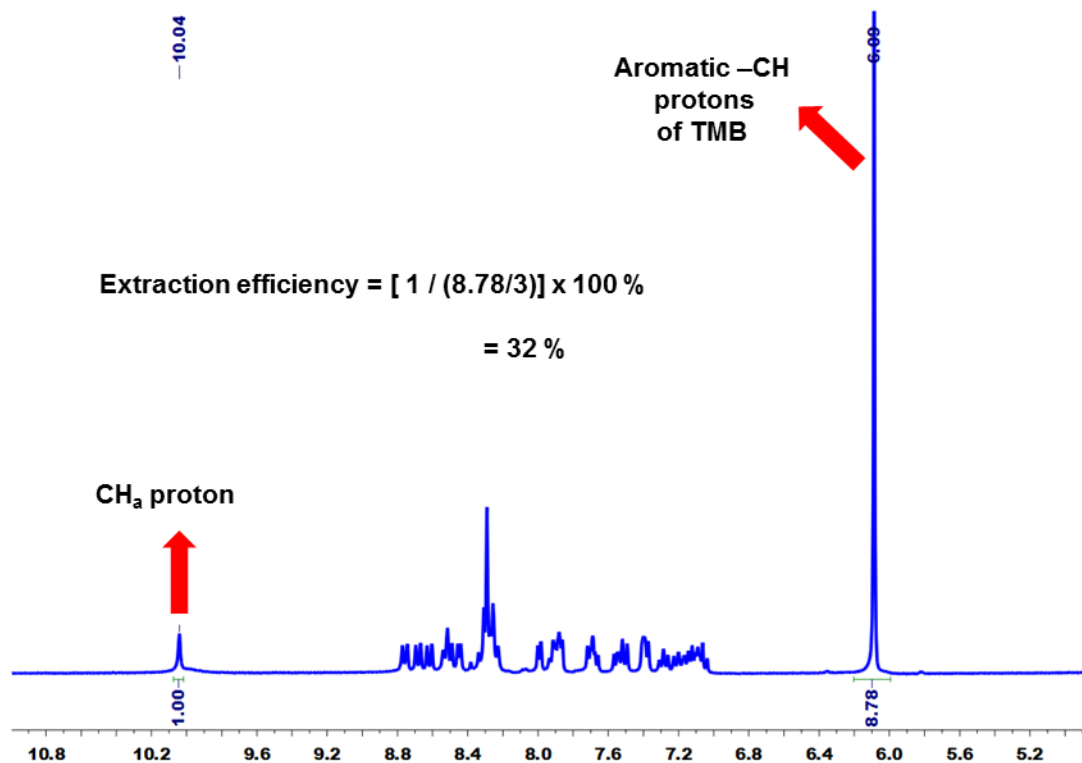


Figure S49. Calculation of extraction efficiency of complex $1[\text{PF}_6]_2$ with TBAH_2PO_4 via liquid-liquid extraction, using TMB as an internal standard.

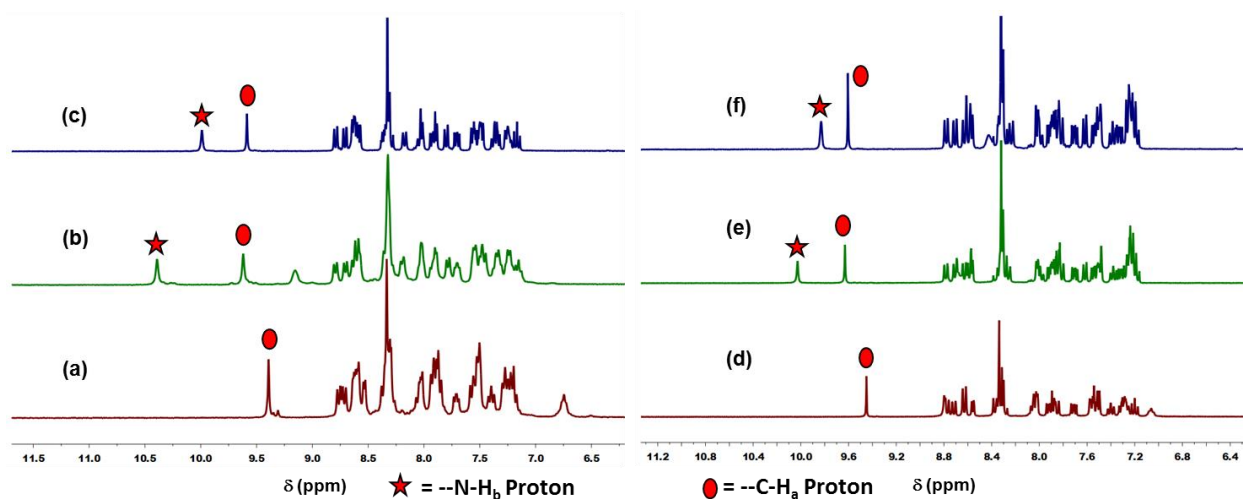


Figure S50. ^1H NMR spectra of (a) complex $1[\text{PF}_6]_2$, (b) 1:1 mixture of complex $1[\text{PF}_6]_2$ and $\text{TBAO}_2\text{CCH}_3$, (c) extracted complex from liquid-liquid extraction between complex $1[\text{PF}_6]_2$ and $\text{TBAO}_2\text{CCH}_3$, (d) complex $2[\text{PF}_6]_2$ (e) 1:1 mixture of complex $2[\text{PF}_6]_2$ and TBAO_2CPh , (f) extracted complex from liquid-liquid extraction between complex $1[\text{PF}_6]_2$ and TBAO_2CPh .

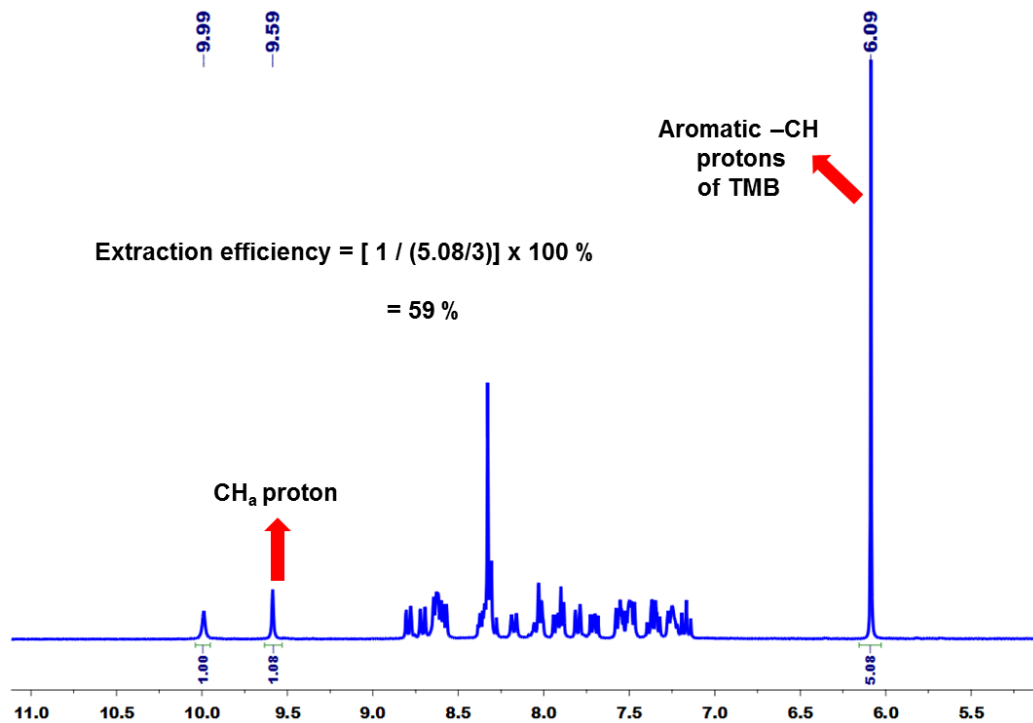


Figure S51. Calculation of extraction efficiency of complex **1**[PF₆]₂ with TBAO₂CCH₃ *via* liquid-liquid extraction, using TMB as an internal standard.

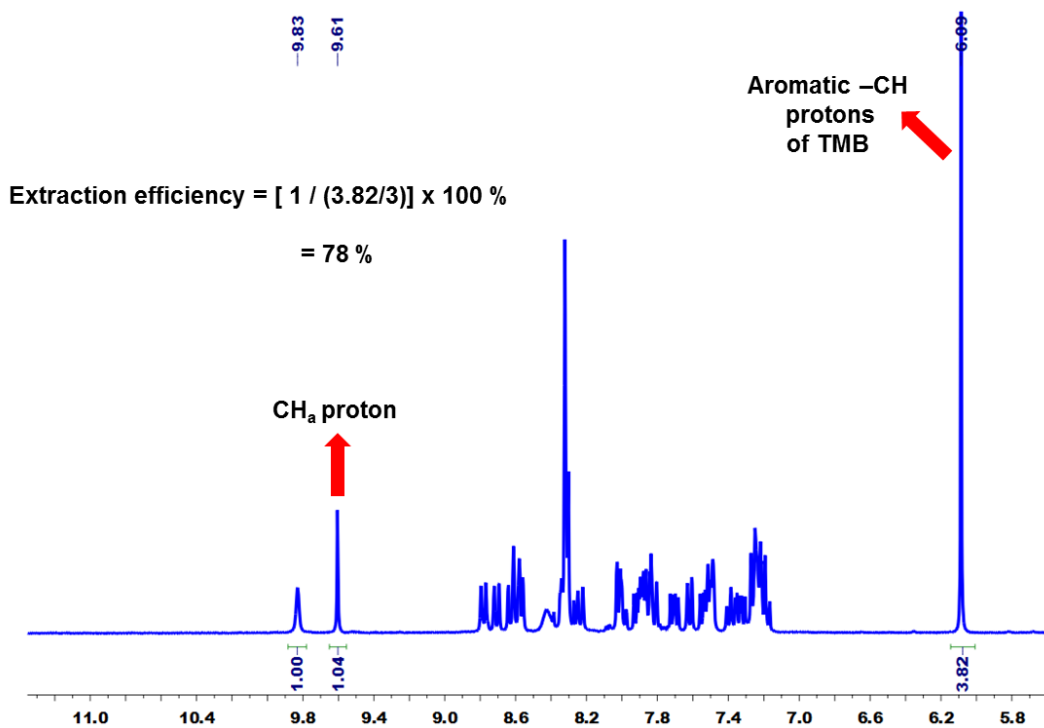


Figure S52. Calculation of extraction efficiency of complex **1**[PF₆]₂ with TBAO₂CPh *via* liquid-liquid extraction, using TMB as an internal standard.

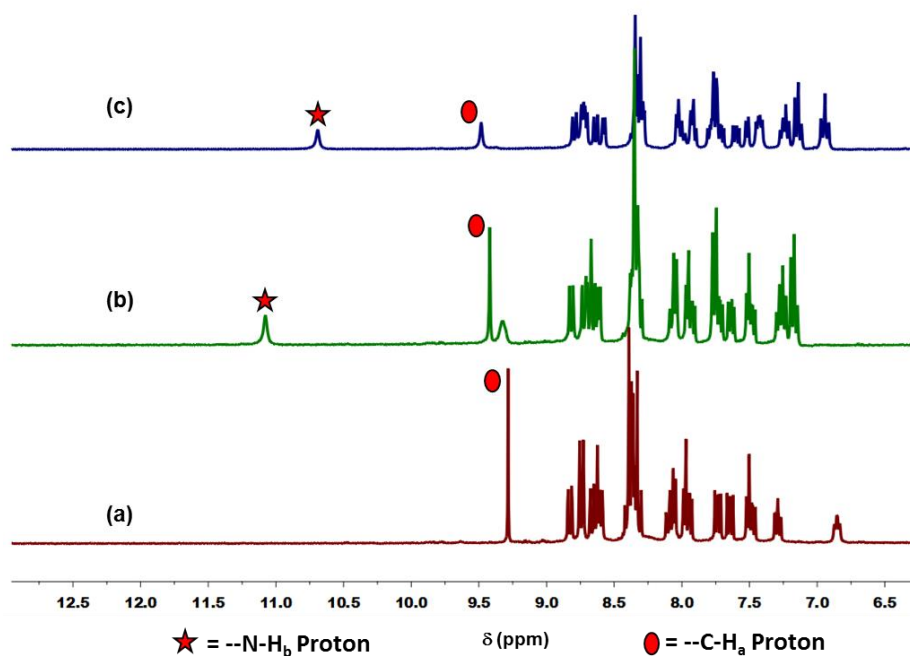


Figure S53. ^1H NMR spectra of (a) complex $2[\text{PF}_6]_2$, (b) 1:1 mixture of complex $1[\text{PF}_6]_2$ and TBAO_2CPh , (c) extracted complex from liquid-liquid extraction between complex $1[\text{PF}_6]_2$ and TBAO_2CPh .

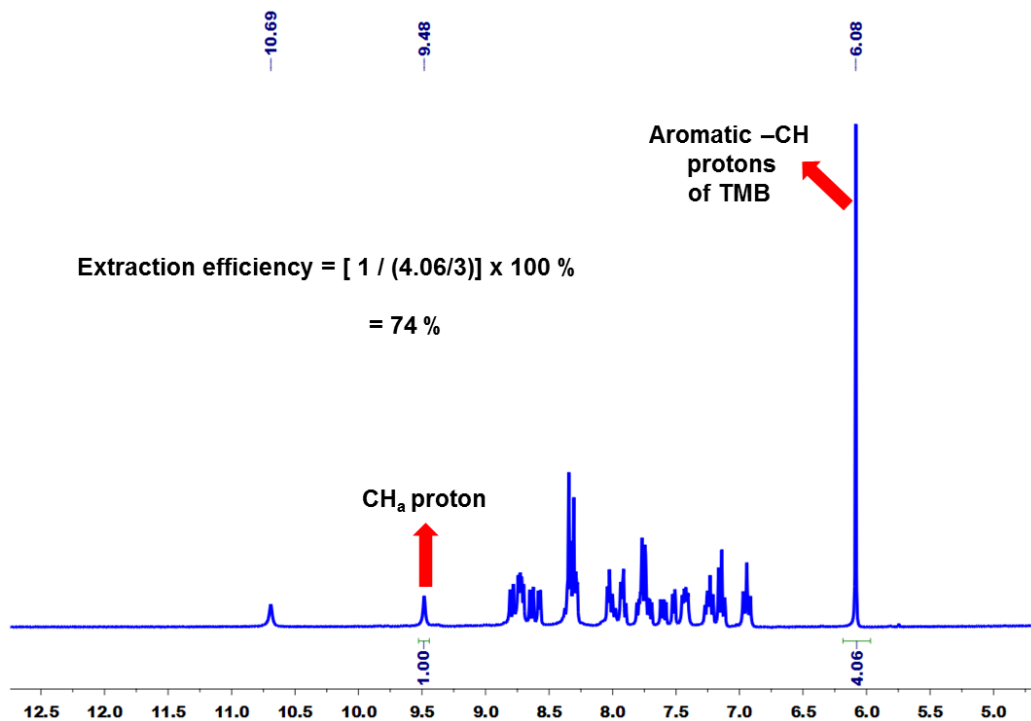


Figure S54. Calculation of extraction efficiency of complex $2[\text{PF}_6]_2$ with TBAO_2CPh via liquid-liquid extraction, using TMB as an internal standard.

References:

1. (a) S. K. Chauthe, R. J. Sharma, F. Aqil, R. C. Gupta and I. P. Singh, *Phytochem. Anal.*, 2012, **23**, 689-696; (b) T. Rundloef, M. Mathiasson, S. Bekiroglu, B. Hakkarainen, T. Bowden and T. Arvidsson, *J. Pharm. Biomed. Anal.*, 2010, **52**, 645-651.
2. E. Pershagen, J. Nordholm and K. E. Borbas, *J. Am. Chem. Soc.*, 2012, **134**, 9832-9835.
3. J. E. Collins, J. J. S. Lamba, J. C. Love, J. E. McAlvin, C. Ng, B. P. Peters, X. Wu and C. L. Fraser, *Inorg. Chem.*, 1999, **38**, 2020-2024.
4. M. J. Hynes, *J. Chem. Soc., Dalton Trans.*, 1993, 311-312.
5. (a) D. Brynn Hibbert and P. Thordarson, *Chem. Commun.*, 2016, **52**, 12792-12805; (b) P. Thordarson, *Chem. Soc. Rev.*, 2011, **40**, 1305-1323.
6. (a) P. D. Beer and P. A. Gale, *Angew. Chem., Int. Ed.*, 2001, **40**, 486-516; (b) F. P. Schmidtchen and M. Berger, *Chem. Rev.*, 1997, **97**, 1609-1646.